EPJ manuscript No.
(will be inserted by the editor)

RADs energetics and constraints on emerging tori collisions around super-massive Kerr Black Holes

D. Pugliese[1] and Z. Stuchlík[2]

Institute of Physics and Research Centre of Theoretical Physics and Astrophysics, Faculty of Philosophy&Science, Bezručovo náměstí 13, CZ-74601 Opava, Czech Republic

Received: date / Revised version: date

Abstract. We provide constraints on possible configurations and interactions of two coplanar tori orbiting a central Kerr black hole (BH), in dependence on its dimensionless spin. The two-tori configurations can be directly linked to the current models featuring the obscuration of galactic BH X-ray emission. The emergence of each torus instability phases is discussed and tori collision has been also investigated. The first simple evaluation of the center-of-mass energy proves that collision-energy-efficiency increases with the dimensionless BH spin. We explore the phenomenological aspects of the corotating and counterrotating tori by analyzing properties of the orbiting toroidal configurations related to the fluid enthalpy flux, the mass-flux, the mass-accretion-rates, and the cusp luminosity in the two cases of corotating and counterrotating fluids in dependence on the SMBH spin. The analysis resulted ultimately in a comparative investigation of the properties of corotating versus counterrotating tori, demonstrating that two accretion tori can orbit around the central Kerr attractor only under very specific conditions. Our results also demonstrate that the dynamics of the unstable phases of these double tori systems is significant for the high energy phenomena which could be observable in the X-ray emission and extremely energetic phenomena in active galactic nuclei and quasar.

PACS. XX.XX.XX No PACS code given

1 Introduction

Observations in the X-ray emission are on the verge of the astrophysical development in the high energy sector and in many senses we can safely say that thay contribute significantly to make a challenging period for astrophysics. Surely, the planned new satellite observatories represent expected breakthrough mission in this sector[1] [1]. Consequently, theoretical models are continuously challenged by new data that require new emerging hypotheses supported by computational simulations by appropriately adapted numerical integration codes. There is then a remarkable area which is potentially capable to unify very different issues of high energy astrophysics connecting X-ray emission, black hole **(BH)** physics related to accretion processes, and galaxy mergers see, e.g., [2] and [3,4]. The origin of X-ray emission in **BH** environments is especially viewed as accretion related, and possibly a bridge between galaxy and a galactic **BH** activity keeping fingerprints of galaxy mergers[5, 6,7,8,9,4,10]. There are various studies of the X-ray emission profile, and more generally jet emission, using more or less the general scheme of the emission "screened" by some "bubbles" of matter configurations in equilibrium, assumed to be located in the inner region between the **BH** and an outer disk orbiting the central attractor. We mention also obscuring torus in Galaxy X-ray emission [12,13,14,15] and [16], for a discussion on the role of the inner and outer part of an accretion disk [17]. In fact, active galactic nuclei **(AGN)** "obscuration" is generally linked to some toroidal configurations possibly surrounding the **AGN** accretion disk [18,19,20,21]. The results we found in the present paper should be directly comparable with investigation of **AGN**-**BH** X-ray spectra. We set opaque geometrically thick toroidal surfaces that are likely produced during **BH** growth due to "clumpy" episodic accretion processes, implying potentially interesting consequences on the X-ray emission and oscillations in the black hole accretion systems–see also [22,23, 24,25] for different charged models of structured disks.

Motivated by these facts, in the present work we consider the possibility to provide reliable general constraints for any "adjoint" orbiting structures which may serve as a guide to model developments of the accreting systems. We investigate this situation by carefully studying coplanar structured toroidal disks, so called *ringed accretion disks* (**RADs**), first introduced in [26] and then detailed in [27,28,30,31]. The set-up for the ringed accretion disk model was drown in [27], where constraints and discussion on perturbations were provided. Then in [28] sequences of unstable configurations were discussed, the investigation was focused on the unstable phases of accreting

Send offprint requests to:

[1] For example from **XMM-Newton**: `https://www.cosmos.esa.int/web/xmm-newton`, to NASA's **Chandra** X-ray Observator: `http://cxc.harvard.edu/index.html`, **NuSTAR** (Nuclear Spectroscopic Telescope Array) `http://www.nustar.caltech.edu/page/about` and **Swift BAT** (Burst Alert Telescope) `https://swift.gsfc.nasa.gov/about_swift/bat_desc.html`.

multi toroidal structures. The paper [29] focused on the case of two tori as "seed" for larger configurations. The **RAD** configurations were then discussed in more detailed form in two works[32,30]. The fourth fundamental study of the **RAD** is related to their energetics and it is subject of the present paper. We provide indication on the doubled toroidal structures that can be detected independently on the attractor characteristic spin and, as a sideline result, we also explicitly present first evaluation of the efficiency of the tori collisions and energy release in **RADs** colliding tori. Our results show that even in the simplest but effective set-up considered here, the presence of such "screening bubbles" cannot be considered as a general universal property of any spinning attractor, but on the contrary, the systems composed by orbiting multi structures (within the symmetry conditions fixed here) must undergo strict constraints on the relative tori rotation and they strongly depend on the dimensionless spin of the central Kerr attractor. This result remarkably sets, for the first time to our knowledge, a strong unifying framework for studying of an orbiting multiple configuration and its **BH** attractor [30]. Specifically, we show that only four **BHs** classes, distinguished according to their dimensionless spin, can host specific **RAD** configurations, in dependence on periods of the life of the attractor and the **RAD**. This finding thus represents a precise guidance and gives directions to orient any studies featuring possible screening effects in this framework. The constraints provided here are very restrictive– we argue that, by considering different processes leading to **RAD** formation, some **RAD** configurations are likely to be formed around some specific attractors in some periods of the **RAD-BH** life[30,27,28,32,33].

From the observational point of view, the phenomenology associated with these toroidal complex structures can be very wide. Our studies could open up a new field of investigation in astrophysics, leading us to reinterpret various phenomena analyzed so far in the single torus framework. In the new framework, requiring the possibility of multi-tori systems, we can simultaneously revisit the actual analysis of screened X-ray emission by considering constraints provided here. The related observational evidence may be gained by the spectral features of **AGNs** X-ray emission line shape, due to the X-ray obscuration and absorption by one of the tori. In [34,35] and [36, 37], for instance, it was proposed that the **AGNs** X-ray spectra should provide a fingerprint of the tori: relatively indistinct excesses of the relativistically broadened emission-line components were predicted, arising in a well-confined radial distance in the accretion structure originating by a series of episodic accretion events. Thus, hints of formation processes are also briefly addressed.

The **RADs** feature systems made up of several axis-symmetrical matter configurations orbiting in the equatorial plane of a single central Kerr **BH**. In the model development, and especially in the choice for **RAD** toroidal components, we have taken into account that tori may be formed during several accretion regimes occurred in the lifetime of non-isolated Kerr **BHs**. Indeed, formation of several accretion tori orbiting one central super-massive Kerr black hole (**BH**) has been conjectured specifically as a peculiar feature of **AGNs** and Quasars-[26,27,28, 38,34,35,36,37,39]. Therefore, evidences of these special configurations are expected to be found in the associated X-ray spectra emission in **AGNs**. In these environments, tori might be formed as remnants of several accretion regimes occurred in various phases of the **BH** life and could eventually be reanimated in non-isolated systems where the central attractor is interacting with the environment, or in some kinds of binary **BH** systems[40,41,42]. Some additional matter could be supplied into the vicinity of the central **BH** due to tidal distortion of a star, or if some cloud of interstellar matter is captured by the strong gravity [43,44]. During evolution of **BHs** in these environments both corotating and counterrotating accretion stages are mixed in various accretion periods of the attractor life [45, 46,47]. For the construction of a reliable model, this makes it necessary to consider, for a rotating central attractor, the possibility of different orientation of the spin for several aggregations of matter orbiting the attractor, and to consider this possibility in the associated phenomena. We will show that remarkably for some attractors only counterrotating tori could be considered as inner screening object.

From methodological view-point, it is clear that **RAD** investigation is affected by a series of challenging issues. This rather complex scenario envisages different aspects of black hole and accretion torus life subject to numerous and articulated studies. The existence of different evolution periods of the **BH**-**RAD** systems should be carefully considered in any model construction requiring several assumptions on the **BH-RAD** history according to the different scenarios of the force balance of the torus in each period. To fix our idea we may conveniently introduce the following three **RAD**-periods: **I**- period features tori formation, **II**-period consists in the torus accretion onto the central Kerr attractor and finally a **III**-period deals with tori interaction and tori collision emergence. Here we mainly focus on period **(II)**, discussing the unstable configurations as defined in this analysis, and period **(III)**, by considering conditions for the emergence of tori collisions, providing very simple approximative evaluation for the collision energy release.

The morphology of each component of the **RAD** is a fat torus in equilibrium, centered on the attractor. This is an example of opaque (large optical depth) and super-Eddington (high matter accretion rates) model: a radiation pressure supported accretion torus, cooled by advection with low viscosity. The development of this model was firstly drawn up by Abramowicz and his collaborators in a series of works [48,49,50,51, 52] and then adopted in different contexts: particularly this is today widely adopted as the initial conditions in the set up for simulations of the GRMHD (magnetohydrodynamic) accretion structures [53,54,55,56,57]. Consequently, the adaptability and common use of this model in much more complex dynamical scenarios has driven our choice towards the application for each **RADs** component, taking care to guide our investigation into results on the ranges of variation of the relevant quantities. The individual toroidal (thick disk) configurations are prescribed by barotropic models, for which the time scale of the dynamical processes τ_{dyn} (regulated by the gravitational and inertial forces) is much lower than the time scale of the thermal ones τ_{therm} (heating and cooling processes, radiation) that is lower than the time scale of the viscous processes τ_ν; thus $\tau_{dyn} \ll \tau_{therm} \ll \tau_\nu$ and the effects of strong gravitational fields are dominant with respect to the dissipa-

tive ones and predominant to determine the unstable phases of the systems [58,52,26,49], see also [59,54,55,60,61,62,63, 64]. As a consequence, during the dynamical processes, the functional form of the angular momentum and entropy distribution depends on the initial conditions of the system and on the details of the dissipative processes. Paczyński realized that it is physically reasonable to assume ad hoc distributions. This feature constitutes a great advantage of these models and render their adoption extremely useful and predictive. The tori are governed by "Boyer's condition" of the analytic theory of equilibrium configurations of rotating perfect fluids [65]. The toroidal structures of orbiting barotropic perfect fluid are determined by an effective potential reflecting the spacetime geometry, and the centrifugal force component through the distribution of the specific angular momentum $\ell(r)$ of the orbiting fluid – [26,66,67,64,68,69,70,71,72,73,74,56,75]. The entropy is constant along the flow and, according to the von Zeipel condition, the surfaces of constant angular velocity Ω and of constant specific angular momentum ℓ coincide [76,77,78] (this implies in particular that the rotation law $\ell = \ell(\Omega)$ is independent of the equation of state [64,79]). Consequently the perfect fluid equilibrium tori are regulated in a given spacetime by the specific angular momentum distribution function $\ell(r)$, and a *constant* K, related to the fluid effective potential, determining the matter content of the tori. The equipressure surfaces, K =constant, could be closed, determining equilibrium configurations, or open (proto-jet configurations related to jets [28, 31]). The special case of cusped equipotential surfaces allows for accretion onto the central black hole [51,48,49,52]. The outflow of matter through the cusp occurs due to an instability in the balance of the gravitational and inertial forces and the pressure gradients in the fluid, i.e., by the so called Paczynski mechanism of violation of mechanical equilibrium of the tori [48].

The **RADs** model is based on several symmetry assumptions on the tori-central attractor system. In fact, in our approach we take full advantage of the symmetry of the Kerr geometry, considering a stationary and axisymmetric, full general relativistic (GR) model for a single thick accretion disk with a toroidal shape; a generalization to different symmetry misaligned disk and even tilted disk may be convened in future work as a modification of the general case considered here. Thus we address directly the question, if two aligned axi-symmetric accretion tori can orbit a central coplanar Kerr attractor. The response to this issue provided in this work is positive: a double tori may orbit and even accrete around a central Kerr **BH**. However, this may occur only in four special cases, constrained by the dimensionless spin of the central attractor, the tori specific angular momentum and the relative rotation of the two tori. The tori evolution may lead to the interaction and eventual destruction of the tori system. We briefly discuss conditions for these critical phenomena emergence, providing an evaluation of the center-of-mass energy for colliding fluid particles originating in both tori.

Tori may collide and merge or eventually turn to origin some *feeding–drying* processes with some possible interesting phenomenological consequences on the periodical radiation emission: the accreting matter from the outer torus can impact on the inner torus located between the outer one and the central **BH**, or the outer torus may be inactive with an active inner torus accreting onto the **BH**, or both tori may be accreting [27,28]; for tidal destruction see [3]. Radially oscillating tori could be also related to the high-frequency quasi periodic oscillations observed in non-thermal X-ray emission from compact objects [80]. We expect therefore that future analysis should throw new light on those aspects of the dynamical processes not covered by our first analysis.

Following the three previous papers related to various aspects of the **RAD** model, we present here a fourth paper of this series, devoted to the energetics of the **RAD** and constraints of collisions of tori constituting the **RADs**.

The plan of this article is as follows: we summarize the basic properties of stationary toroidal fluid configurations in Kerr spacetime in Sec. (2), where the system formed by the pair of tori is also introduced. The construction of the **RAD** tori aggregate led to the introduction of new notations adapted to the new concepts, most of which are suited to represent the agglomerate as a whole accreting disk. In Sec. (2) a general review of the model is provided, the main notation related to the new concepts are listed in Table (1). Our analysis leads to certain number of sideline results, considering especially the possibility of counterrotating accreting tori orbiting a central Kerr **SMBH**. While this subject has been developed in literature, we had to specify in the **RAD** framework some more details of the tori features performing a comparative analysis of the main features of the counterrotating tori with respect to the corotating tori. We report in the Sec. (3) results concerning the tori morphology (tori edges and elongation on the equatorial plane) for these two classes of tori, considering very carefully the different behavior in relation to the **BH** spin according to different values of the model parameters, in particular the magnitude of the fluid specific angular momentum. Throughout this analysis we also clarify some aspects constraining the emerging of the tori collisions. In Sec. (4) we discuss the occurrence of tori collisions: constraints are provided in Sec. (4.1) while in Sec. (4.2) we provide an evaluation of center-of-mass energy for two colliding particles from the two interacting tori. In Sec. (4.3) we focus our investigation directly on the phenomenological aspects of the corotating and counterrotating tori. We analyze quantities defining the fluid enthalpy flux, the mass-flux, the mass accretion rates, and the cusp luminosity in the two cases of corotating and counterrotating fluids in dependence on the **SMBH** spin, the fluid specific angular momentum, and further parameters related to the fluid density. Sec. (4.4.1) includes some considerations on the polytropic fluids considered in our framework. Finally we close this article in Sec. (5) presenting a general discuss on collisional phenomena in the **RAD** from a more global perspective, considering the case of tori in accretion. Concluding remarks follow in Sec. (6), where future perspective of our investigations is also provided. Appendix (A) specifies details on the role of the frame-dragging in the ergoregion of the Kerr geometry, in relation to the accreting tori of the **RAD**.

2 Axi-symmetric tori in a Kerr spacetime

We consider two axially symmetric tori with symmetry plane coinciding with the equatorial plane of the central Kerr **BH** of

mass parameter M and dimensionless spin $a/M \in [0,1]$ [27,28, 26,52,66]. The Kerr metric tensor can be written in the Boyer-Lindquist (BL) coordinates $\{t, r, \theta, \phi\}$ as follows

$$ds^2 = -\frac{\Delta - a^2\sin^2\theta}{\rho^2}dt^2 + \frac{\rho^2}{\Delta}dr^2 + \rho^2 d\theta^2 + \frac{\sin^2\theta\left(\left(a^2+r^2\right)^2 - a^2\Delta\sin^2\theta\right)}{\rho^2}d\phi^2 \quad - 2\frac{a\sin^2(\theta)\left(a^2-\Delta+r^2\right)}{\rho^2}d\phi dt\,,$$
$$\rho^2 \equiv r^2 + a^2\cos\theta^2, \quad \Delta \equiv r^2 - 2Mr + a^2. \tag{1}$$

The horizons $r_- < r_+$ and the outer static limit r^+_ϵ are respectively given by:

$$r_\pm \equiv M \pm \sqrt{M^2 - a^2}; \tag{2}$$
$$r^+_\epsilon \equiv M + \sqrt{M^2 - a^2\cos\theta^2}; \tag{3}$$

there is $r_+ < r^+_\epsilon$ on $\theta \neq 0$ and $r\_\epsilon^+ = 2M$ in the equatorial plane, $\theta = \pi/2$–[84]. The extreme Kerr black hole has spin-mass ratio $a/M = 1$, while the non-rotating limiting case $a = 0$ is the Schwarzschild metric. As the line element (1) is independent of ϕ and t, the covariant components p_ϕ and p_t of a particle four–momentum are conserved along the geodesics, therefore[2] the quantities

$$E \equiv -g_{\alpha\beta}\xi^\alpha_t p^\beta, \quad L \equiv g_{\alpha\beta}\xi^\alpha_\phi p^\beta\,, \tag{4}$$

are constants of motion, where $\xi_t = \partial_t$ is the Killing field representing the stationarity of the Kerr geometry and $\xi_\phi = \partial_\phi$ is the rotational Killing field.

The constant E for timelike geodesics represents the total energy of the test particle coming from radial infinity, as measured by a static observer at infinity, while L is the axial component of the angular momentum of the particle. The Kerr metric (1) is invariant under the application of any two different transformations: $x^\alpha \to -x^\alpha$ for one of the coordinates (t, ϕ), or the metric parameter a, and the test particle dynamics is invariant under the mutual transformation of the parameters $(a, L) \to (-a, -L)$. This makes possible to limit the analysis of the test particle circular motion to the case of positive values of a for corotating ($L > 0$) and counterrotating ($L < 0$) orbits with respect to the black hole [81,82,83].

We focus here on the case of a one-species particle perfect fluid (simple fluid), described by the energy momentum tensor

$$T_{\alpha\beta} = (\varrho + p)u_\alpha u_\beta + \ pg_{\alpha\beta}, \tag{5}$$

where ϱ and p are the total fluid density and pressure, respectively, as measured by an observer moving with the fluid whose four-velocity u^α is a timelike flow vector field. Due to symmetries of the problem, we always assume $\partial_t \mathbf{Q} = 0$ and $\partial_\varphi \mathbf{Q} = 0$, $\mathbf{Q}$ being a generic spacetime tensor. The fluid dynamics is described by the *continuity equation* and the *Euler equation* respectively:

$$u^\alpha\nabla_\alpha\varrho + (p+\varrho)\nabla^\alpha u_\alpha = 0$$
$$(p+\varrho)u^\alpha\nabla_\alpha u^\gamma + \ h^{\beta\gamma}\nabla_\beta p = 0, \tag{6}$$

where the projection tensor $h_{\alpha\beta} = g_{\alpha\beta} + u_\alpha u_\beta$ and $\nabla_\alpha g_{\beta\gamma} = 0$ [26, 84]. We investigate the fluid toroidal configurations centered on the plane $\theta = \pi/2$, and defined by the constraint $u^r = 0$. No motion is assumed also in the θ angular direction ($u^\theta = 0$). Considering a barotropic equation of state $p = p(\varrho)$, the continuity equation is identically satisfied as consequence of the conditions, while from the Euler equation in (6) we find

$$\frac{\partial_\mu p}{\varrho + p} = -\partial_\mu W + \frac{\Omega\partial_\mu\ell}{1-\Omega\ell}; \quad W \equiv \ln V_{eff}(\ell), \tag{7}$$
$$\text{where} \quad V_{eff}(\ell) = u_t = \pm\sqrt{\frac{g^2_{\phi t} - g_{tt}g_{\phi\phi}}{g_{\phi\phi} + 2\ell g_{\phi t} + \ell^2 g_{tt}}},$$

Ω is the relativistic angular frequency of the fluid relative to the distant static observers, and $V_{eff}(\ell)$ provides an *effective potential* for the fluid, assumed here to be characterized by a conserved and constant specific angular momentum ℓ (see also [64,79]).

Similarly to the case of the test particle dynamics, the function $V_{eff}(\ell)$ in Eq. (7) is invariant under the mutual transformation of the parameters $(a, \ell) \to (-a, -\ell)$, therefore we can limit the analysis to positive values of $a > 0$, for *corotating* ($\ell > 0$) and *counterrotating* ($\ell < 0$) fluids and we adopt the notation ($\pm$) for counterrotating or corotating matter respectively. Therefore, the accretion tori corotate ($-$) or counterrotate ($+$) with respect to the Kerr **BH**, for $\ell_\mp a \gtrless 0$ respectively. As a consequence of this, considering the case of two orbiting tori, (i) and (o) respectively, we need to introduce the concept of ℓ*corotating* tori, $\ell_i\ell_o > 0$, and ℓ*counterrotating* tori, $\ell_i\ell_o < 0$. The ℓcorotating tori can be both corotating, $\ell a > 0$, or counterrotating, $\ell a < 0$, with respect to the central Kerr attractor [27].

On the other hand, the specific angular momentum distribution of circular geodesics governs the ringed accretion disk

$$\ell_\pm(r;a) \equiv \frac{L}{E} = \tag{8}$$
$$= \frac{a^3M + aMr(3r-4M) \pm \sqrt{Mr^3\left[a^2 + (r-2M)r\right]^2}}{[Ma^2 - (r-2M)^2 r]M},$$

namely centers (and cusps) of the individual tori.

Note that the constant specific angular momentum ℓ in Eq. (7), characterizing each toroid of the **RAD**, is related to the "geodesic angular momentum distribution" $\ell_\pm(r;a)$ of Eq. (8), due to the fact that for a fixed $r = \bar{r}^\pm > r^\pm_{mso}$, the value $\ell_\pm(\bar{r}^\pm;a)$ provides the specific angular momentum ℓ of the torus centered in $\bar{r}^\pm$, see also [52].

The tori are regulated by the balance of the hydrostatic and centrifugal factors due to the fluid rotation and by the curvature effects of the Kerr background, encoded in the effective potential function V_{eff}.

[2] We adopt the geometrical units $c = 1 = G$ and the $(-,+,+,+)$ signature, Greek indices run in $\{0,1,2,3\}$. The four-velocity satisfy $u^a u_a = -1$. The radius r has unit of mass $[M]$, and the angular momentum units of $[M]^2$, the velocities $[u^t] = [u^r] = 1$ and $[u^\varphi] = [u^\theta] = [M]^{-1}$ with $[u^\varphi/u^t] = [M]^{-1}$ and $[u_\varphi/u_t] = [M]$. For the seek of convenience, we always consider the dimensionless energy and effective potential $[V_{eff}] = 1$ and an angular momentum per unit of mass $[L]/[M] = [M]$.

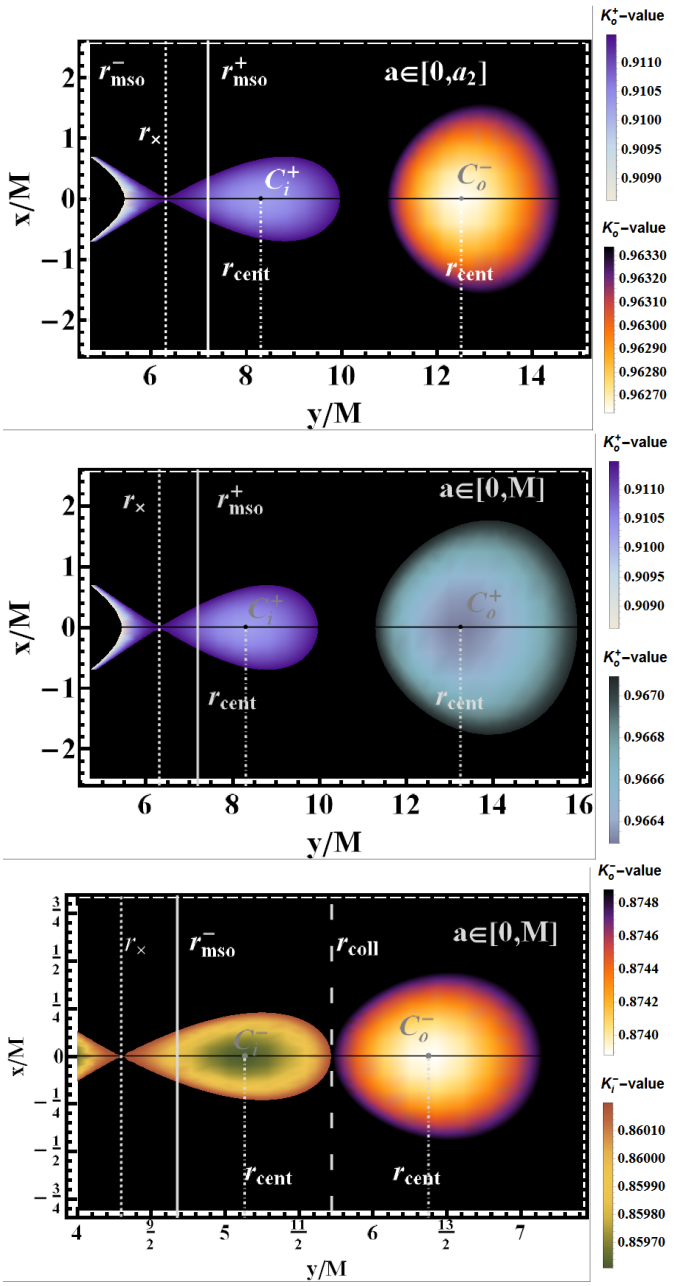

Fig. 1. GRHD numerical 2D integration of Eq. (7) for the couples $C_\times^+ < C^-$ (upper panel), $C_\times^\pm < C^\pm$ (center and bottom panel), orbiting a central Kerr **BH** attractor with spin $a = 0.382M$, (x, y) are Cartesian coordinates. Tori centers r_{cent}, tori collision point r_{coll}, and inner edge of accreting tori are also shown. See also Fig. (14).

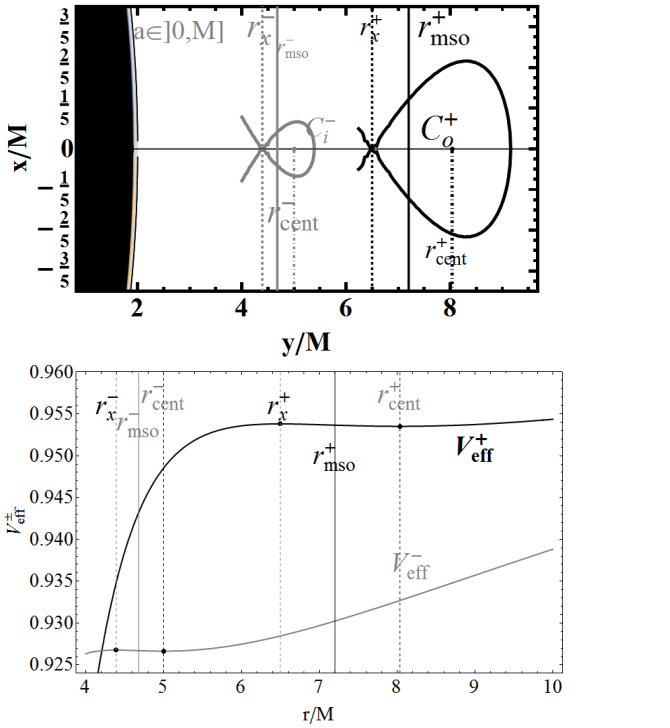

Fig. 2. *Upper panel*: Cross sections on the equatorial plane of the outer Boyer surfaces Roche lobes for ℓcounterrotating tori $C_\times^- < C_\times^+$ (as there is $r_{cent}^- < r_{cent}^+$, and there is $C_\times^- <_\times C_\times^+$ for it is $r_\times^- < r_\times^+$) orbiting a central Kerr **BH** attractor with spin $a = 0.382M$, (x, y) are Cartesian coordinates and fluid specific angular momentum $\ell^- = 3.31$, $\ell^+ = -3.99$, parameters $K^- = 0.927516$ and $K^+ = 0.953141$. *Bottom panel:* Effective potential V_{eff} as function of r/M. This special tori couple is investigated also in Figs (4) (5), (14)-bottom and (11).

The procedure adopted in the present article borrows from the Boyer theory on the equipressure surfaces applied to a torus [65,56], where the Boyer surfaces are given by the surfaces of constant pressure or[3] Σ_i =constant for $i \in (p, \varrho, \ell, \Omega)$, [65,66], where the angular frequency is indeed $\Omega = \Omega(\ell)$ and $\Sigma_i = \Sigma_j$ for $i, j \in (p, \varrho, \ell, \Omega)$. Many features of the tori dynamics and morphology like their thickness, their stretching in the equatorial plane, and the location of the tori are predominantly determined by the geometric properties of spacetime via the effective potential V_{eff}. The boundary of any stationary, barotropic, perfect fluid body is determined by an equipotential surface, i.e., the surface of constant pressure (the Boyer surface) that is orthogonal to the gradient of the effective potential. The toroidal surfaces are the equipotential surfaces of the effective potential $V_{eff}(\ell)$, considered as function of r, solutions $\ln(V_{eff}) = c$ = constant or $V_{eff} = K$ =constant. The couple of parameters (ℓ, K) uniquely identifies each Boyer surface–Figs (2). It should also be noted that, according to Eq. (7), the maximum of the hydrostatic pressure corresponds to the minimum of the effective potential V_{eff}, and it is the torus center r_{cent}. The instability points of the tori, as envisaged by the P-W mechanics, are located at the minima of the pressure and therefore maximum of V_{eff}—Figs (2). To identify these points, we therefore need to compute the critical points of $V_{eff}(r)$ as function of the radius r. Equation $\partial_r V_{eff}$ can be solved for the specific angular momentum of the fluid $\ell(r)$–Fig. (3).

In fact, the forces balance condition for the accretion torus can be encoded in two functions defining each **RAD** component: the torus fluid (critical) specific angular momentum: $\ell_{crit}^\pm(a; r)$: $\partial_r V_{eff} = 0$, defining the critical points of the hydrostatic pressure in the torus, see Eq. (8) and the function $K_{crit}^\pm(a; r, \ell)$:

[3] More generally $\Sigma_{\mathbf{Q}}$ is the surface **Q** =constant for any quantity or set of quantities **Q**.

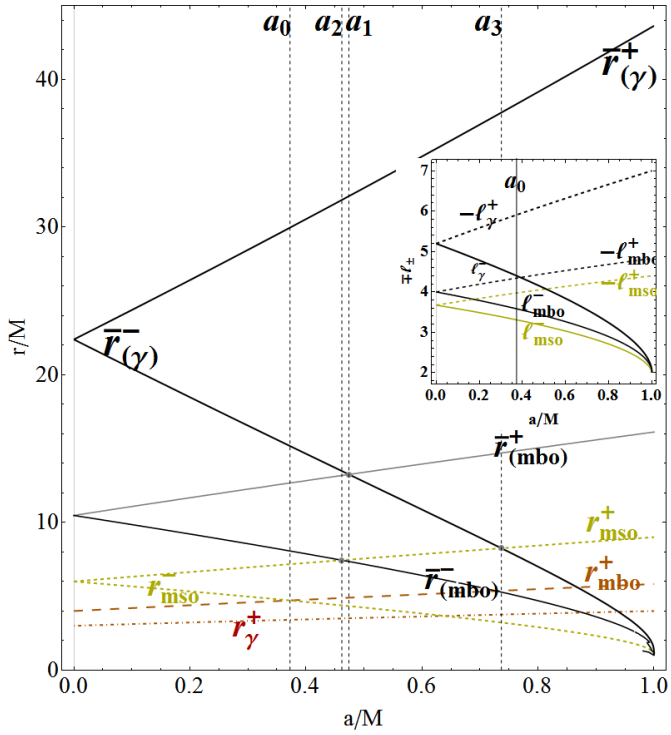

Fig. 3. Radii $\{\bar{r}^{\pm}_{(\gamma)}, \bar{r}^{\pm}_{(mbo)}, \bar{r}^{\pm}_{(mso)}\}$ versus $a/M \in [0,1]$. Spins $\{a_1, a_2, a_3\}$, introduced in Eq. (11), and a_0 introduced in Sec. (4.2) are also shown. The marginally stable circular orbit $r^{\pm}_{mso}$, the marginally bounded circular orbit $r^{\pm}_{mbo}$ and finally the marginal (photon) circular orbit r^{+}_{γ}, for counterrotating (+) and corotating (-) fluids are also shown. *Inside panel*: Fluid specific angular momentum $\{\ell^{\pm}_{\gamma}, \ell^{\pm}_{mbo}, \ell^{\pm}_{mso}\}$ as function of the dimensionless spin $a/M \in [0,1]$.

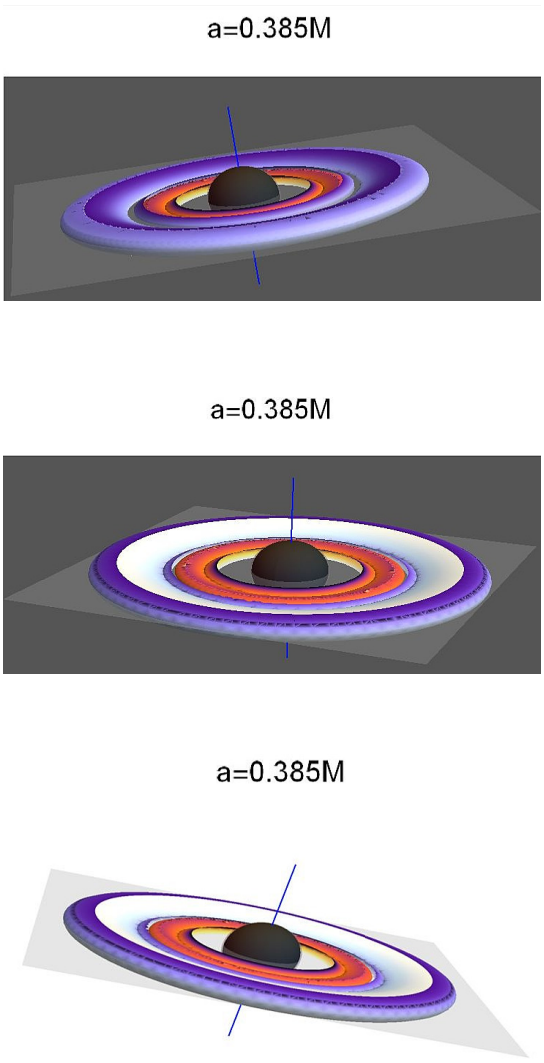

Fig. 4. GRHD-Numerical 3D integration of tori density surfaces (solutions of Eq. (7)). Colors are chosen according to improved visual effects. Integration is stopped at the emerging of tori collision. Black region is $r < r_+$, r_+ is the outer horizon of the Black hole of spin $a = 0.385M$, gray region is the outer ergosurface. *Top panel* pictures two ℓcounterrotating tori $C^{-}_{\times} < C^{+}_{\times}$, the inner corotating torus and the outer counterrotating torus is accreting onto the central **BH**, accretion flux is stopped during **RAD** integration. *Center panel* focuses on a different **RAD** view, to focus on the region close to the **BH** and to colliding region. *Bottom panel* shows a second collision phase when the matter flow from the outer counterrotating torus impacts on the inner corotating accreting torus. Tori, centered on the **BH**, are coplanar and orbiting on the equatorial plane of the central Kerr **BH**. The *entire* **SMBH-RAD** system is tilted relative to the observer.

$V_{eff}(a; r, \ell^{\pm}_{crit})$, for counterrotating and corotating fluids respectively, ℓ_{crit} is present as a fundamental feature of the theory of accretion disks [52]. In the following, we use ℓ and K generally as model parameters and parameter values, while ℓ_{crit} and K_{crit} are the functions of a/M and r. We consider these functions extensively in the following. Functions $\{\ell^{\pm}_{crit}(a; r), K^{\pm}_{crit}(a; r)\}$ have been of great methodological importance in the development of the **RAD** model [27], through the definition of the set of the functions $\{\ell^{i}_{crit}\}^{n}_{i=1}$, $\{K^{i}_{crit}\}^{n}_{i=1}$ (the **RAD** order n is the number of its components) which is also the basis for the definition of effective potential of the agglomerate [27]. In the model adopted for each component of the **RAD** considered here, the specific angular momentum of the torus lies on a set of level surfaces $\ell^{i} = \ell^{i}_{crit}(a; r)$ =constant, as the parameter $K^{i} = K^{i}_{crit}(a; r)$ =constant. Functions $\{\ell^{\pm}_{crit}, K^{\pm}_{crit}\}$ are pictured in Figs 5–while further considerations are reflected in Figs 6 and Figs 11. Curves $K^{\pm}_{crit}(a; r, \ell)$ locate the tori centers, provide information on torus elongation (see Fig. 7) and density and, for a torus accreting onto the central **BH**, determine the inner and outer torus edges. Angular momentum $\ell^{\pm}_{crit}(a; r)$ does *not* coincide with the Keplerian momentum L, describing the free particle angular momentum, but it is related to this function through Eq. (8)–an extensive discussion on the role of L and ℓ in the accretion tori and accretion processes can be found in [26,67], while $\ell^{\pm}_{crit}(a; r)$ and $K^{\pm}_{crit}(a; r)$ have been widely investigated in the developing of the **RAD** model in [27,29]. Our investigation is focused on the task to find the ranges of variation of the main fluid features, as the specific angular momentum, or fluid density related to the K parameter, during different evolutionary phases of the **RAD**: from formation, growth, to accretion of its components and tori collisions. This aspect

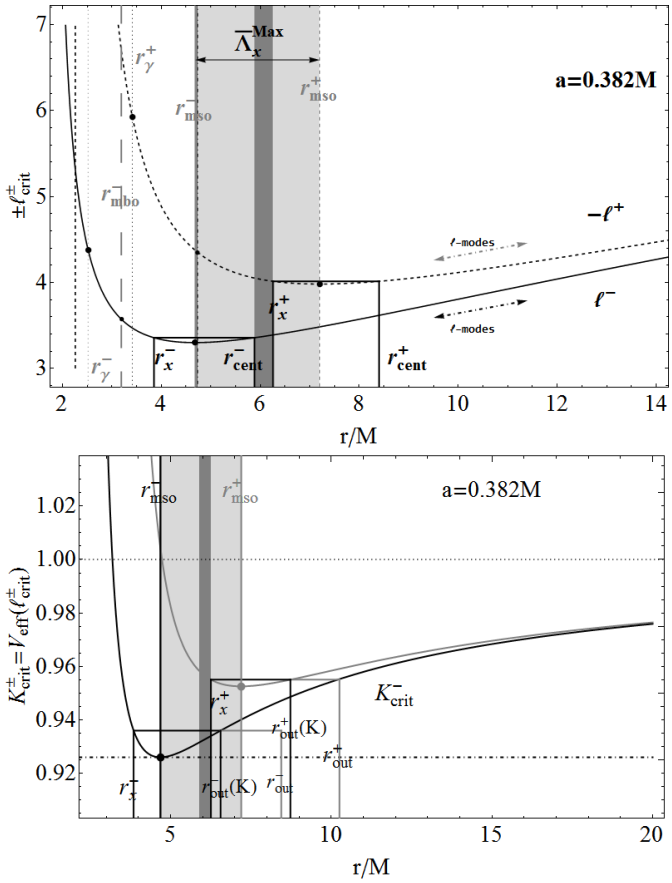

Fig. 5. ℓ-modes representation. *Upper panel*: fluid specific angular momenta $\mp\ell^{\pm}_{crit}$ for counterotating and corotating tori respectively, indicating the pressure extreme points, in the spacetime of a **BH** with spin $a = 0.382M$ as function of r/M. The **RAD** perturbation ℓ–modes reduces to shifts on the each curve $\ell^{\pm}$. Tori centers, $r^{\pm}_{cent}$, and accreting points $r^{\pm}_{\times}$ of a tori couple $C^{-}_{\times} < C^{+}_{\times}$ are shown (lines ℓ =constant), $r^{\pm}_{\gamma}$ are the photon circular orbits–see Figs (4,2) and Fig. (11) for related density surfaces. Light-gray region is the limiting maximum spacing of the two accreting tori in this spacetime, black continuum lines are the marginally stable orbits $r^{\pm}_{mso}$, the gray region is the limiting, maximum spacing for the specific tori in the couple, for growing K_{ℓ}-modes of the inner corotating tori–see also Figs (12) and (13). *Bottom panel*: Plot of $K^{\pm}_{crit}$ as function of r/M, inner edge $r^{\pm}_{\times}$ and outer edges of accreting tori for a colliding couple are also shown, collision region is enlarged. Light-gray region is the maximum limiting *spacing* for the two accreting tori. each torus elongation on the equatorial plane is set by the K_{crit} =constant lines. Gray shades the same region as in upper-panel. Note that for an accreting torus plots $K_{crit}(r)$ do not directly locate the torus center, neither can be easily related to the effects of ℓ or K-modes. For non accreting (quiescent) tori, lines $K_{crit}(r)$ =constant locate the inner edge of an accreting torus $r_{\times}$ and the *center* r_{cent} (in figure $r_{out}(K)$) an ℓcorotating couple of tori with different angular momentum, see for a throughout discussion and main applications [27]. Figs (11) and Figs (6) for further details. Limiting values $K^{-}_{mso} < K_{\rm lim} \equiv 1$ are represented by dot-dashed and dotted lines respectively.

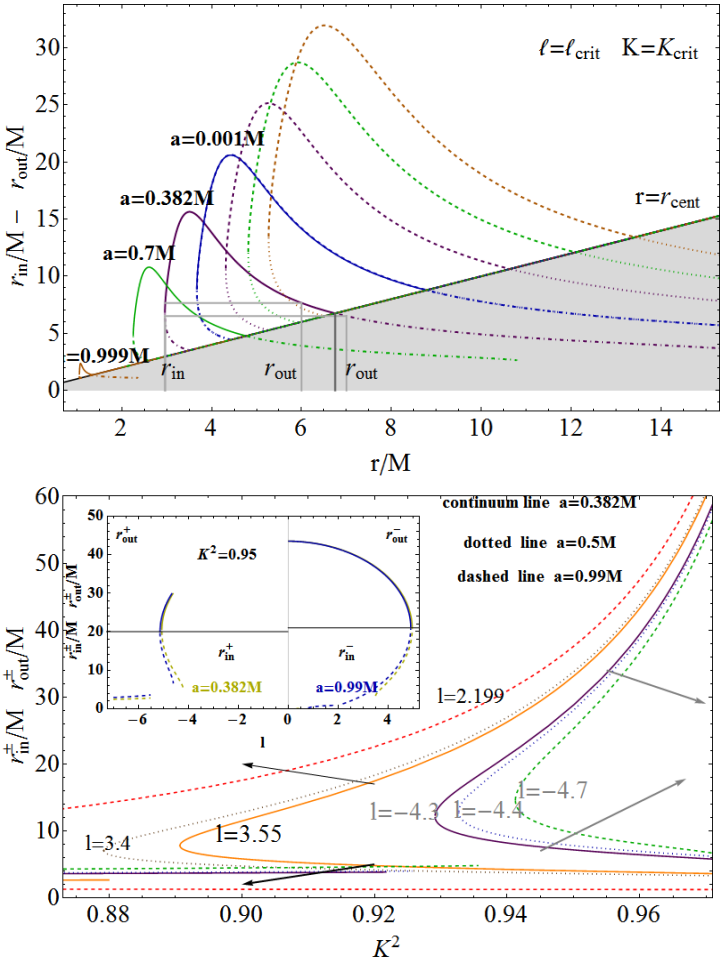

Fig. 6. *Upper panel*: plots of the inner r_{in} and outer r_{out} edges of **RADs** accretion tori orbiting different **SMBHs** (spins a on curves), as functions of r/M. r_{in} and r_{out} are introduced in Eqs (14). Shaded region is $r < r_{cent}$, r_{cent} is the line of torus centers where at fixed r/M there is $r_{cent} = r$. Corotating tori are represented in continuum and dotdashed curves, thick dashed and thick dotted curves are for counterrotating tori. Horizontal lines on each curve fix a torus (constant angular momentum), torus inner and outer edges are signed on the figure–see discussion on Eq. (14). *Bottom panel*: Inner $r^{\pm}_{in}$ and outer edges $r^{\pm}_{out}$ of accretion torus, at different spins and fluid specific angular momentum for corotating (**-**) and counterrotating (**+**) fluids. as functions of K^2 where $K \in [K_{mso}, 1[$. Arrows follow increasing values of the **SMBHs** spins. Inside panel: radii $r^{\pm}_{in}$ and edges $r^{\pm}_{out}$ as functions of specific angular momentum ℓ, for corotating and counterrotating fluids, for **SMBH** spins $a = 0.99M$ and $a = 0.382M$ at $K^2 = 0.95$.

allows a general applicability of the results found here eventually to other accreting disk models for the aggregate components. We will briefly resume this argument concerning tori collisions in Sec. (4.3). In general model of accretion disks the angular momentum of matter in accretion disks is considered to be sufficiently high for the centrifugal force to be a predominant component of the four forces regulating the disks balance (centrifugal, gravitational, pressure and magnetic forces), the Bondi quasi-spherical accretion constitutes an example of situation when the condition ($|\ell| > |L|$) is not fulfilled. In gen-

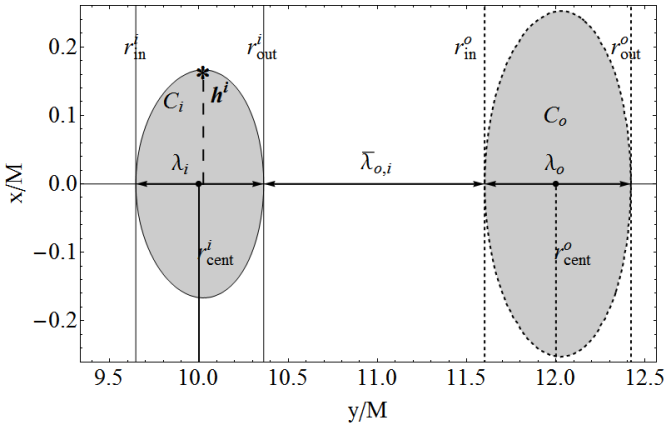

Fig. 7. Cross sections on the equatorial plane of the consecutive Boyer surfaces of two separated rings $C_i < C_o$, with boundaries ∂C_i and ∂C_o, the tori centers $r_{min} = r_{cent}$ are signed with points and the lines r_{cent} =constant. With $r/M = \sqrt{x^2+y^2}$ and (x, y) are Cartesian coordinates. The inner r_{in} and outer r_{out} edge are also signed, λ_a for $a \in \{i, o\}$ are the tori elongation and $\bar{\lambda}_{o,i}$ is the spacing among the tori. h^i is the height associated to the C_i torus, or the maximum point of the surface ∂C_i The ℓcorotating rings, rotate around a black hole attractor with spin $a = 0.75M$ and specific angular momentum $\ell_i = -4.2897$ and $\ell_o = -4.41883$.

eral accretion disks, there must be an extended region where there is $\mp\ell^{\pm} > \mp L^{\pm}$ (explicitly considering also the counterrotating fluids) in the same orbital region. This is assumed to hold for a general accretion torus with a general angular momentum distribution. In this work we provide limit to the inequality $|L| < |\ell|$ according to different conditions set on the **RAD**. Then, a particularly attractive feature of tori with constant specific angular momentum ℓ is that the ℓcorotating tori and particularly ℓcounterrotating tori are constrained by the Kerr geometry *geodesic structure*[4]: this comprise the *marginally stable circular orbit*, $r^{\pm}_{\rm mso}$, the *marginally bounded circular orbit*, $r^{\pm}_{\rm mbo}$ and the *marginal circular orbit* (photon orbit) $r^{\pm}_{\gamma}$-Fig. (3). It is also necessary to introduce also the radii $r^{\pm}_{(\rm mbo)}$ and $r^{\pm}_{(\gamma)}$, defined as the solutions of the following equations:

$$(-)\ r^{\pm}_{(\rm mbo)}:\ \ell_{\pm}(r^{\pm}_{(\rm mbo)}) = \ell_{\pm}(r^{\pm}_{\rm mbo}) \equiv \ell^{\pm}_{\rm mbo}, \tag{9}$$

$$(-)\ r^{\pm}_{(\gamma)}: \ell_{\pm}(r^{\pm}_{(\gamma)}) = \ell_{\pm}(r^{\pm}_{\gamma}) \equiv \ell^{\pm}_{\gamma},$$
$$\text{where}\quad r^{\pm}_{\gamma} < r^{\pm}_{\rm mbo} < r^{\pm}_{\rm mso} < r^{\pm}_{(\rm mbo)} < r^{\pm}_{(\gamma)} \tag{10}$$

–see Fig. (3). The radii $r_{(\gamma)}$ and $r_{(mbo)}$ are related to the radii r_{γ} and r_{mbo} through the angular momenta ℓ_{γ} and ℓ_{mbo} respectively. Accordingly, there are the following critical values of the spin:

$$a_1 \equiv 0.4740M:\quad r^{+}_{(\rm mbo)} = r^{-}_{(\gamma)},$$
$$a_2 = 0.461854M:\ r^{-}_{(\rm mbo)} = r^{+}_{\rm mso},$$
$$a_3 \equiv 0.73688M:\ r^{-}_{(\gamma)} = r^{+}_{\rm mso}, \tag{11}$$

see Figs (3). The role of radii $r_{(\gamma)}$ and $r_{(mbo)}$ can be easily seen by considering the lines ℓ =constant on $\ell(r)$ in Fig. (3). It is simple to see that, consistently with most of the axi-symmetric accretion tori models, the *(stress) inner edge* of the accreting torus is at $r_{\times} \in]r_{\rm mbo}, r_{\rm mso}]$, while the torus is centered at $r_{cent} > r_{\rm mso}$ [85,86,87,88]. This consistency with the relevant ranges for most of the accretion tori is a good indication of the reliability of this approach to **RADs** at different systems.

In each couple, the two tori are generally severely constrained in mutual relations of the ranges of variation of fluids specific angular momentum, tori edges location, and the attractor spin: it can be shown that the center of each torus turns to be located in $[r_{mso}, r_{(mbo)}]$, $[r_{(mbo)}, r_{(\gamma)}]$, $r > r_{(\gamma)}$, whereas the inner edge of each torus lies in these ranges or in $[r_{mbo}, r_{mso}]$, in dependence of the range of the parameter ℓ, and if the tori are accreting or non-accreting. Any accreting torus is in fact a toroidal solution of the Euler equation (6) with proper boundary conditions admitting a cusp, a point of hydromechanical destabilization. The vanishing pressure implies a non equilibrium regime at radii $r \leq r_{\times}$ with the consequent dynamical mass loss from the disk induced by the Roche lobe overflow (a self-regulating process for the accretion rate of many kinds of accreting disks–see[52]). The range of fluid specific angular momentum values where closed cusped solutions can be found is restricted to $]\mp\ell^{\pm}_{mso}, \mp\ell^{\pm}_{mbo}[$ respectively for counter-rotating and corotating tori. It is straightforward to show that the location of the *center* (point of fluid maximum hydrostatic pressure and density) is at $r_{cent} \in]r_{\rm mso}, r_{(\rm mbo)}[$. If $\pm\ell^{\mp} > \pm\ell^{\mp}_{\gamma}$, then the torus center is located in $r^{\mp}_{cent} > r^{\mp}_{(\gamma)}$, this torus has no critical configuration (according to P-W mechanism)-[27,28]. We have therefore a way to place the critical pressure points according to the range of variation of the fluid specific angular momentum. We refer to Table (1) which explicitly introduces the ranges **L1**, **L2** and **L3** of the fluid momentum ℓ.

In the following, it will be convenient to use the notation $\mathrm{C}^{\pm}$ ($\mathrm{C}^{\pm}_{\times}$) for non-accreting (accreting) tori, $()^{\pm}$ for a torus which may be non-accreting or accreting (according to hydro-gravitational destabilization due to P-W mechanism [52]). Boyer surfaces and density plots with indication on the relative notation are in Figs (2) and Figs (1).

Also, symbols $\lesseqgtr$ ($\lesseqgtr_{\times}$) for two tori refer to the relative position of the tori centers r_{cent} (accretion points or unstable points $r_{\times}$): thus, for example, we use short notation $(()^{-} < ()^{+}, ()^{-} <_{\times} ()^{+}) \equiv ()^{-} \ll_{\times} ()^{+}$ that means $r^{-}_{cent} < r^{+}_{cent}$ and $r^{-}_{\times} < r^{+}_{\times}$–see Figs (2) and Table (1).

We can proceed now by solving the hydrodynamic equations (7) with a barotropic equation of state associated to each torus of the four couples $()^{\pm}_{i} < ()^{\pm}_{o}$ and $()^{\pm}_{i} < ()^{\mp}_{o}$, respectively within the conditions $r^{o}_{in} \geq r^{i}_{out}$ for the inner r^{o}_{in} (outer (r^{i}_{out})) edge of the outer (inner) torus. Here the fluid specific angular momentum varies in the ranges $\ell \in [\ell_{mso}, \ell_{mbo}]$, $[\ell_{mbo}, \ell_{\gamma}]$ or $\ell > \ell_{\gamma}$. We refer to Table (1) for a brief summary of the introduced notation including brief description. The analysis can be then further simplified by considering appropriate boundary conditions on a properly defined effective potential for the couple of tori. In fact, we may introduce, as in [27], an effective potential $V^{\mathrm{C}^2}_{eff}\big|_{K}$ and also alternative $V^{\mathrm{C}^2}_{eff}$ potential for the

[4] It is worth specifying that this strong dependence of the model on the geometric properties of spacetime induced by the central attractor enables us to apply to a certain extent the results found here to different models of accretion disks [52].

system of the two tori

$$V^{\mathbf{C}^2}_{eff}\Big|_K \equiv V^i_{eff}\Theta(-K_i)\bigcup V^o_{eff}\Theta(-K_o)$$
and
$$V^{\mathbf{C}^2}_{eff} \equiv V^i_{eff}(\ell_i)\Theta(r^o_{cent}-r)\Theta(r-r_+)\bigcup V^o_{eff}(\ell_o)\Theta(r-r^i_{cent}),$$

where Θ is the Heaviside (step) function such that for example $\Theta(-K_i) = 1$ for $V^i_{eff} < K_i$ and $\Theta(-K_i) = 0$ for $V^i_{eff} > K_i$. The constraints in $V^{\mathbf{C}^2}_{eff}$ are provided through the parameters $\{K_i, K_o\}$, while the potential $V^{\mathbf{C}^2}_{eff}$ is determined by the fixed centers (r^i_{cent}, r^o_{cent}) only. The effective potential of the couple can therefore be written as a coupling of the effective potentials for each torus. In both cases, with $V^{\mathbf{C}^2}_{eff}$ and $V^{\mathbf{C}^2}_{eff}\Big|_K$, the two tori are determined by the couple of the parameters K_i =constant and K_o =constant (where ℓ_i and ℓ_o are fixed).

The results show that two non-accreting ℓcorotating and ℓcounterrotating tori might orbit any Kerr attractor, if their specific angular momenta are properly related. However, the emergence of accretion occurs in the following four couples only:

$$\begin{aligned} &\textbf{(i)}:\ \mathrm{C}^{\pm}_{\times} < \mathrm{C}^{\pm}, \quad \textbf{(ii)}:\ \mathrm{C}^{+}_{\times} < \mathrm{C}^{\pm}, \\ &\textbf{(iii)}:\ \mathrm{C}^{-}_{\times} < \mathrm{C}^{\pm}, \quad \textbf{(iv)}:\ \mathrm{C}^{-}_{\times} < \mathrm{C}^{+}_{\times} \end{aligned} \tag{12}$$

see Figs (2) and Figs (1).

We can describe results as it follows: for a ℓcorotating couple ((**i**)), or a Schwarzschild (*static* ($a = 0$)) attractor, only the inner torus of a couple can be accreting (this can be also seen by considering the curves ℓ=constant for $\ell(r)$ Fig. (3)-right).

In the ℓcounterrotating case, an accreting *corotating* torus must be the inner one of the couple while the outer counterrotating torus can be non-accreting or in accretion-Fig. (2).

If there is a $\mathrm{C}^{-}_{\times}$ torus, or if the attractor is static, then no inner (corotating or counterrotating) torus can exist, and then $\mathrm{C}^{-}_{\times}$ is part of $\mathrm{C}^{-}_{\times} < \mathrm{C}^{-}$ couple as in Figs (1) or of a $\mathrm{C}^{-}_{\times} < ()^{+}$ one as in Figs (2), that is the inner accreting torus of a couple where the outer is quiescent (in this case it can be corotating or counterrotating) or also in accretion and in this case it has to be counterrotating.

A corotating torus can be the outer of a couple of tori with an inner counterrotating accreting torus. Then the outer torus may be corotating (non accreting), or counterrotating in accretion or non-accreting–Figs (1). Both the inner corotating and the outer counterrotating torus of the couple can accrete onto the attractor. A counterrotating torus can therefore reach the instability being the inner one of a ℓcorotating or ℓcounterrotating couple as in Figs (2), or the outer torus of a ℓcounterrotating couple as shown in Figs (1).

Then it is worth noting that if the *accreting* torus is *counterrotating* with respect to the Kerr attractor, i.e. a $\mathrm{C}^{+}_{\times}$, then there is *no* inner counterrotating torus, but a couple may be formed as a $\mathrm{C}^{+}_{\times} < \mathrm{C}^{\pm}$ or as a $()^{-} < \mathrm{C}^{+}_{\times}$ one.

Couples $\mathrm{C}^{\pm}_{\times} < \mathrm{C}^{\pm}$ and $\mathrm{C}^{-}_{\times} < \mathrm{C}^{+}$ having only the inner torus in accretion, while the outer torus is *quiescent*, may form around any attractors with $a \in [0, M]$. A $\mathrm{C}^{-}_{\times} < \mathrm{C}^{+}_{\times}$ couple, featuring the occurrence of double accretion, as shown in Figs (2), is possible in all Kerr spacetimes where $a \neq 0$. However, the couple is subjected to several constraints on the fluid specific angular momentum: if the **BH** dimensionless spin $a \lessapprox a_1$, and the lower must be the specific angular momentum ℓ^- of the inner corotating torus. Thus, if a counterrotating torus is accreting onto the central black hole, there could be an inner corotating torus, which may also accrete onto the spinning attractor, acting as a screening torus for the matter flow of the accreting counterrotating outer torus. However, the lower is the Kerr black hole dimensionless spin, say $a \lessapprox a_1$, the lower must be the corotating torus specific angular momentum–see [29]. Nevertheless, a counterrotating torus can therefore reach the instability being the inner or the outer ring of an ℓcounterrotating couple. In fact, couples $()^{+} < \mathrm{C}^{-}$, with an outer corotating and quiescent torus, have to be observed in any spacetime $a \in [0, M]$, but only for slower spinning **BHs** with $a \in [0, a_2[$, the corotating non-accreting (quiescent) torus C^{-} approaches the instability (i.e. the inner edge is $r_{\times} \gtrapprox r^{-}_{\mathrm{mso}}$). Note that the faster is the Kerr attractor ($a \gtrapprox a_3$), the farther away should be the outer torus to prevent collision (i.e. the torus center $r_{cent} > r^{-}_{(\gamma)}$). The system consisting of an inner accreting counterrotating torus and an outer equilibrium corotating torus may be formed in any spacetime, but the faster is the attractor, the farther away should be the outer torus and this also implies the outer torus has large specific angular momentum [27,28,32,33,30]. Finally, we emphasize that for the tori couples with inner corotating tori, in particular for the cases (**ii**) and (**iii**) considered in Eq. (12), the possibility of penetration of matter into ergoregion Σ^{+}_{ϵ}, or the formation of extended toroidal matter configurations contained in this region, can occur; we refer to [26,89,27,28, 32,30,31] for a detailed discussion on this possibility, while in Sec. (A) we briefly add further considerations on this aspect.

General comments on methods We close this section with some methodological notes, introducing next section (4) dealing with tori collisions. In the investigation of **RAD** agglomerate and its internal dynamics, from its formation and evolution to the **RAD** tori collisions, we have taken into account *all* the evolutive possibilities of the model through the parameter analysis, constraining ultimately the **RADs** order and the distribution of momentum depending on the central **SMBH** spin [27, 30]. Here, having fixed the **RAD** order as $n = 2$, we still have different degrees of freedom provided by the K and ℓ parameters; we will better look at this aspect in Sec. (4.1) introducing the **RAD** ℓ-modes and K-modes–[27]. More specifically, as also mentioned above, tori collisions and **RAD** formation are strongly constrained by the geodesic structure of the Kerr spacetime, this fact has been highly emphasized in [27,28,29]. This feature constitutes indeed a methodological advantage of the model, as these limits, because of their geometric nature due to the spacetime properties of the central **BH** attractor, have in fact a major role in determining the force balance in the **RAD** in even more complex situations where, for example, other effects are taken into account, as the magnetic field distribution, which makes these models highly predicting as emerges in agreements with of many GRMHD analysis. Considerations developed here considerably constrain some important features of the an accretion tori formation [32,28], and the possibility of the formation of a tori agglomerate. A further significant consequence is that such kind of investigation provides *ranges* of variation of certain parameter set. For the tori collisions to oc-

Table 1. Lookup table with the main symbols and relevant notation used throughout the article.

C	cross sections of the closed Boyer surfaces (quiescent non accreting torus)
$C_\times$	cross sections of the closed cusped Boyer surfaces (accreting torus)
$O_\times$	cross sections of the open cusped Boyer surfaces (proto-jet)
()	any of the topologies $(C, C_\times, O_\times)$
(r_{in}, r_{out})	inner and outer edge of C_i ring
$\pm$	counterrotating/ corotating
ℓcounterrotating /ℓcorotating tori	$()^\pm - ()^\mp$ /$()^\pm - ()^\pm$ tori
r_{cent}	center of outer Roche lobe (torus center)
$r_\times$	accretion point (stress inner edge of accreting torus)
$r_\jmath$	unstable point in open configurations
r_{coll}	contact point in collisions among two quiescent tori
$r^\pm_{(\mathrm{mbo})}, r^\pm_{(\gamma)}$	radii of the complement geodesic structure in Eq. (9)
L1 (or $\mathbf{L1}^\pm$)	specific angular momentum range: $\mp\ell^\pm \in [\mp\ell^\pm_{mso}, \mp\ell^\pm_{mbo}[$
L2 (or $\mathbf{L2}^\pm$)	specific angular momentum range: $\mp\ell^\pm \in [\mp\ell^\pm_{mbo}, \mp\ell^\pm_{\gamma}[$
L3 (or $\mathbf{L3}^\pm$)	specific angular momentum range: $\mp\ell^\pm \geq \ell^\pm_\gamma$
$\lesssim$	rings sequentiality according to the centers r_{cent} (inner/outer tori) i.e. $r^i_{cent} \lesssim r^i_{cent}$
$()^i, ()^o$	generally inner and outer configurations of a couple i.e. $()^i < ()^o$
$\lesssim_\times$	rings sequentiality according to the critical points $(r_\times, r_\jmath)$ i.e. $r^i_\times \lesssim r^i_\times$
$\ell_{i/i+1} \equiv \ell_i/\ell_{i+1}$	ratio in specific angular momentum of C_i and C_{i+1}
$\mathbf{C}_{coll}/\hat{r}$	colliding couple with r_{coll} located on a radius $\hat{r}$ outer: torus is quiescent
$\mathbf{C}_\times$	colliding couple: the outer torus is accreting
$\mathbf{C}^\times_{coll}$	colliding couple: combination of the two processes $(\mathbf{C}_{coll}, \mathbf{C}_\times)$, where $r^i_{out} = r^o_\times = r_{coll}$
$\mathbf{C}_\times/r^+_{\mathrm{mso}}$	colliding couple: the outer torus is accreting where $r^+_\times \equiv r^+_{\mathrm{mso}}$
$\mathbf{C}_\times/r^+_{\mathrm{mbo}}$	colliding couple: the outer torus is accreting where $r^+_\times \equiv r^+_{\mathrm{mbo}}$

cur, we have to fix parameter values for one specific situation represented by (arbitrarily chosen) initial data, $(\ell_i, \ell_o, K_i, K_o)$, for the tori couple orbiting a specific **SMBHs** with fixed dimensionless spin parameter a/M. The spacetime geodesic structure and its complement structure as defined in Eq. (9), as founded in [27,28] in the developing of the **RAD** model, actually influence the aggregate composition through the function ℓ_{crit}. We note that in the **RAD** context the two functions $(\ell^i_{crit}, \ell^o_{crit})$ must be simultaneously considered in the study of the couple. Figures (5), (2), (12) and (13) well show the different situations for corotating and counterrotating fluids, while further details on this aspect are explored in Sec. (3). The analysis of fluid specific angular momentum ranges solves only a part of the problem to constraint the **RAD**, because together with ℓ_{crit}, it is necessary to consider $K^\pm_{crit}$, and more generally the values of K-parameters which fix in fact many important accretion tori features, from the elongation in the equatorial plane being related to tori density and, for example the mass-accretion-rate– see Sec. (3). The conditions on the collisions have much freedom, depending, at fixed a/M, on the couple (ℓ, K) for the two tori. From a methodological viewpoint, we have reduced the freedom represented by the choice of ℓ and K parameter for any **RAD** component, by using constraints on the fluids critical pressure points, locating the torus inner edge, r_{in}, the torus center, r_{cent}, and the outer edge, r_{out}. The explicit use of these constraints has been also detailed in [28,32]. However, fixing only one or two of these radii, does not respond to the problem of the construction and constraining of the **RAD** structure and evolution. In order to respond to this issue, the whole set of points generated by each toroidal component of the **RAD**, must be *simultaneously* considered during the analysis of **RAD** constraints (see also the **RAD** function Eq. (12)). In Sec. (4.1), constraints on the collision emergence will be provided. The points $\{r^j_{in}, r^j_{cent}, r^j_{out}\}$, for any torus j of the **RAD**, are then studied in a model defined by $2n + 1$ parameters, where n is the **RAD** order (number of the tori composing the **RAD** aggregate). In this investigation there is $n = 2$ and the model parameters are then given by the pairs $\mathbf{p_i} \equiv (\ell_i, K_i)$ and $\mathbf{p_o} \equiv (\ell_o, K_o)$ and by the dimensionless spin a/M of the central **SMBH**–this is a $4 + 1$ parameters model[5]. To simplify the analysis, it was convenient to introduce the notion of the **RAD** *state*, consisting in the precise arrangement of the following characteristics of the couple: parameters (ℓ_i, ℓ_o) and (K_i, K_o), and relative location of the tori edges, topology (if accreting or non accreting torus), if in collision or not. Then, a ringed disk of the order $n = 2$, with fixed critical topology can be generally in $n = 8$ different states according to the relative position of the centers and rotation: $n = 4$ different states if the rings are ℓcorotanting, and $n = 4$ for ℓcountorrotating rings. Considering also the relative location of points of minimum pressure, then the couple $(()_\mathbf{a} - ()_\mathbf{b})$ with different, but fixed topology, could be in $n = 16$ different states. To this number of possibilities we have to add the different cases generated by the K-modes, resulting in the variation of elongation and thickness of each torus. In this work, we reduce these possibilities–[29]. This study applies also to the case of $n > 2$: the 4 couple in Eqs (12) constitute the **RADs seeds**, and the study of the case of larger **RAD**, with $n > 2$, can be carried out by composing the four couples considered here-[27,28]. In Sec. (4.4.1) the constraints are reformulated

[5] Then, we are actually interested in identifying the *ranges* of variation of the $\{\mathbf{p_i}, \mathbf{p_o}, a/M\}$ parameters, while the exact values of there parameters for one special torus model could be easily found, by fixing a/M and appropriate initial conditions [29].

in terms of fluid density. In Sec. (4), we investigate in detail conditions for the emergence of the collisions of the tori in the cases presented in Eq. (12), considering the relations between the fluid specific angular momentum

3 Tori edges and elongation

Tori elongation on the equatorial plane for the **RAD** ringed structure are illustrated in Figs (7) with other relevant quantities of the tori agglomerates, while in Figs (8) and Figs(9) we show the elongation, and the tori inner and outer edges as functions on torus parameters ℓ and K for corotating and counterrotating fluids. As a sideline result to the **RAD** investigation a comparative analysis of the corotating and counterrotating tori is obtained in dependence of the central Kerr black hole spin-to-mass ratio. The hypothesis that counterrotating tori can be formed around supermassive Kerr **BHs** has already been addressed in literature, for example in [45,46,47,90]. However, we have been carried out here a focused investigation, providing a detailed comparative analysis of the two classes of accreting tori. In the **RAD** framework, some of more intriguing consequences of the presence of ringed structure orbiting the central Kerr **BH** have place for ℓcounterrotating tori, thus in this section we provide a perspective of some important aspects of the counterrotating tori with respect to corotating tori. We address a morphological analysis focusing on the elongation and location of inner edge of corotating and counterrotating tori, these results are important also to fix the **RAD** K and ℓ-modes and the tori collision. In Sec. (4.3) we will consider the mass accretion rates and torus luminosity along with other significant features of the accretion tori for corotating and counterrotating fluids in dependence of the **BH** spin.

Torus elongation λ on the equatorial plane can be written as function of the fluid specific angular momentum and the K-parameter as follows:

$$\lambda(a;\ell,Q) = \frac{2}{3}\left[\sin\left(\frac{\arcsin\upsilon}{3}\right) + \cos\left(\frac{\arccos\upsilon}{3}\right)\right]A,$$

where

$$\upsilon \equiv -\frac{9(Q-1)\left[3Q^2(a-\ell)^2 - 2Q\left(\ell^2 - 3a\ell + 2a^2\right) + a^2\right] + 8}{(Q-1)^3A^3},$$

$$A \equiv \sqrt{\frac{3\ell^2(Q-1)Q - 3a^2(Q-1)^2 + 4}{(Q-1)^2}} \quad \text{and} \quad Q \equiv K^2 \quad (13)$$

dimensionless units, $\lambda \to \lambda/M$ and $a \to a/M$, are considered. Note the dependence from the quantities (K^2-1) and $(\ell - a)$–see also [26]. Figs (8) enlighten the symmetries between the tori of the ℓcounterrotating couples. As expected, the elongation $\lambda^{\pm}$ increases with K^2. However, for fixed K, increasing the dimensionless **BH** spin and decreasing the angular momentum magnitude, there is an increase of the torus elongation for corotating fluids, while λ^+ decreases when matter is counterrotating with respect to the central attractor, corresponding also to an increase of angular momentum magnitude. Generally, at a fixed a/M, larger values of K^2_+ are needed for the counterrotating fluids with respect to the corotating ones,

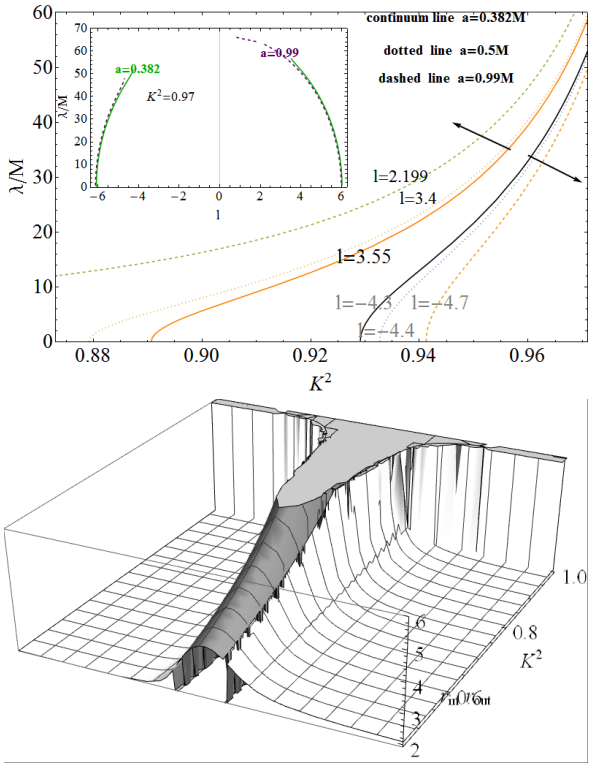

Fig. 8. *Upper panel:* Plots of the tori elongation λ, defined in Eq. (13), for different values of the fluid specific angular momentum and **SMBH** spins as function of the K^2 where $K \in]K^{\pm}_{mso}, 1[$ parameter for counterrotating and corotating tori respectively. Arrows indicate the increasing **BH** spin a/M for the corotating and the counterrotating curves. *Inside panel*, tori elongation λ at fixed K^2, for different **SMBH** spins, as function of fluid specific angular momentum ℓ. It is clear the symmetry of between the ℓcorotating and ℓcounterrotating configurations. *Bottom panel*, torus inner edge r_{in} (white) and outer edge r_{out} (gray) in Eq. (14) as functions of K^2 and fluid specific angular momentum, for **SMBH** spin $a/M = 0.382$.

implying that the counterrotating tori are expected to be characterized generally by larger "density-parameter" K and larger elongation λ then the corotating tori. In Sec. (4.4.1) we shall see how the torus density ϱ and K-parameter can be related; in this way, the results of this analysis set in terms of the K-parameter could be directly read as constraints on the tori fluid density. Figs (8) however represent the two accretion tori, C^+ and C^-, by considering the separation of the two set of curves. The inner panel better shows such symmetry by considering the elongation $\lambda^{\pm}$ versus $\ell^{\pm}$, at fixed K^2, holding for the set of corotating and counterrotating curves included in the frame panel. This analysis also proves the different role played by the **BH** spin for the evolution of the corotating and counterrotating tori: for greater values of the **BH** spin a/M, larger values of K and $|\ell|$ are generally expected. Figs (9) then show better this situation, by focusing on a more accurate analysis of the two different situations represented by the ℓcounterrotating couples and evidencing differences and symmetries of the two toroids. To obtain a comparative analysis between the corotating and counterrotating fluids in dependence of the **BH** spin, we set the specific angular momentum as $\ell^{\mp}_M(a) \equiv \pm(\ell^{\mp}_{mbo} - \ell^{\mp}_{mso})/2$,

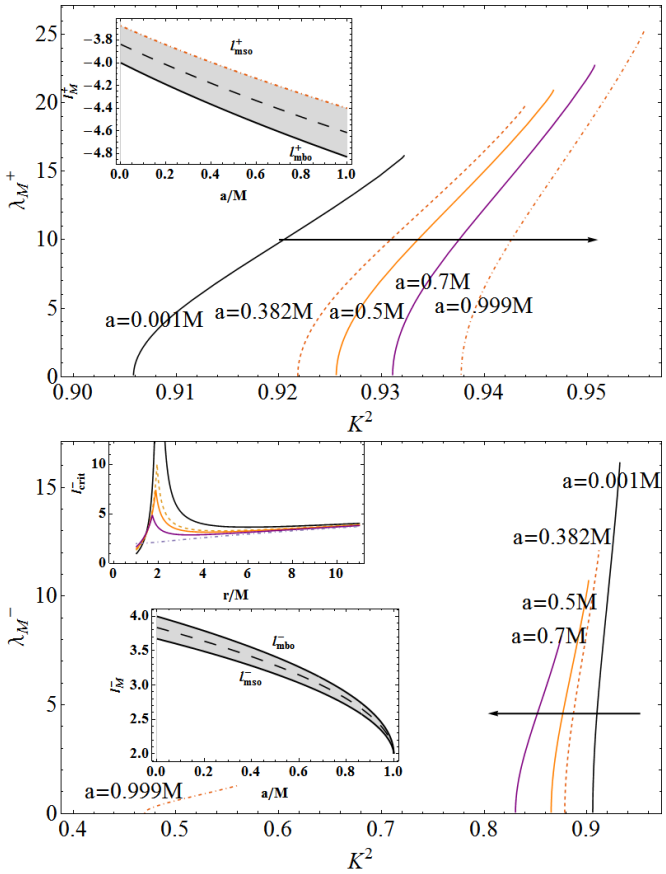

Fig. 9. Torus elongation $\lambda_M(a;\ell_M,K^2)$ in Eq. (13) on the equatorial plane for corotating λ_M^- (*left panel*) and counterrotating fluids λ_M^+ (*right panel*) for fixed values of **SMBH** spin a/M (as singed on each curves) as function of K^2, where $K\in[K_{mso},1[$. Arrows follow increasing values of **SMBHs** a/M. There is $\ell_M^{\mp}\equiv\pm(\ell_{mbo}^{\mp}-\ell_{mso}^{\mp})/2$, dashed black curve in inside panels, gray region sets the the entire range of variation of tori specific fluid angular momentum ℓ depending on the central **SMBH** dimensionless spin a/M, and the range for the function ℓ_{crit}. Right inside panel shows the curves ℓ_{crit}^- as function of a/M.

this is a function of the **BH** spin. Each curve is bounded by the case of a particle string ring (with null elongation) to the limiting open configuration of proto-jet. As expected, the K^+-range lingers in values greater then the K^- parameter, and λ^+ increases with K^+. However, tori with equal elongation may have different angular momentum and they can even orbit **BHs** with different spin-to-mass ratio; as such the tori elongation (with some exceptions for the corotating cases) cannot be used as tracers for the **BH** dimensionless spin or to reveal the tori fluid rotation with respect to the central Kerr attractor. For the counterrotating fluids, increasing the **BH** spin, and following the λ^+ =constant lines, there is an increase of $-\ell^+$ (inner panel) and K^+. At K=constant, on the other hand, some regions of K-values do not allow the tori formation, but with increasing a/M, $-\ell^+$ increases, while the elongation λ^+ decreases. Considering the vertical line at K=constant, the curves for the counterrotating fluids are more spaced with respect to the corotating case. However, in general the elongation can be relatively very large up to $\lambda^+\gtrsim 15M$. Focusing on the analysis for the corotating case, we noted that the curves are more close to each others at small spins, viceversa, there is a pronounced difference between $a=0.7M$ and $a=0.999M$ attractors. This is because the corotating case is, at high **BH** spin, very much dependent on the variation of the **SMBH** spacetime structure, particularly for very high spin the frame-dragging becomes relevant and the tori may approach the ergoregion[6] –see also discussion in Sec. (A). The curves representing the elongation of corotating tori are closer in the $\lambda-K^2$ plane then for the counterrotating ones, this implies, for sufficiently small **BH** spin, a significant similarity of certain characteristics of such tori with respect to parameters K^2, which renders more difficult to distinguish different **SMBH**-**RAD** system. Noticeably, it is possible, however, to distinguish tori orbiting around slow rotating attractor and those around faster rotating Kerr **SMBHs**. The elongation λ^- is generally rather smaller, then the counterrotating case being $\lambda^-\lesssim 14M$. Moreover K^-, ℓ^- and λ^- decrease with a/M, contrary to the counterrotating case The variation of the curves of K^2, with the respect to the counterrotating case, suggests that at fixed a/M, for a small variation of K ($K_\ell-$modes) λ increases rapidly, and this is more clear for the slow rotating **BHs**. These results are finally confirmed also from the the inner panel plots. This is an interesting difference in the ℓcounterrotating tori having potentially significant implications on tori collisions. In the characterization of the ℓcounterrotating systems, these doubled analysis has to be considered simultaneously.

Similarly, we can evaluate the inner and outer edge of an accretion torus as follows:

$$r_{in}(a;\ell,\overline{Q})=-\frac{2}{3}\left[\alpha\cos\left[\frac{1}{3}(\pi+\arccos\beta)\right]+\frac{1}{\overline{Q}}\right],\qquad(14)$$

$$r_{out}(a;\ell,\overline{Q})=\frac{2}{3}\left[\alpha\cos\left(\frac{1}{3}\arccos\beta\right)-\frac{1}{\overline{Q}}\right],$$

where

$$\alpha=\sqrt{\frac{4+3\overline{Q}\left[(\overline{Q}+1)(\ell^2-a^2)+a^2\right]}{\overline{Q}^2}},\qquad(15)$$

$$\beta=-\frac{9\overline{Q}\left[(\overline{Q}+1)(\ell^2-a^2)+a^2\right]+8+27(\overline{Q}+1)\overline{Q}^2(a-\ell)^2}{\alpha^3\overline{Q}^3}\qquad(16)$$

and $\overline{Q}\equiv(K^2-1)<0$

(dimensionless units have been used). Figs (6) and Figs (10) explicitly show the variation of these quantities with respect to the fluid rotation ℓ and the K^2 parameter, a further analysis, showed in Figs (11), pictures a more complex situation featuring the special case of couples $C_\times^-<C_\times^+$, where the dependence of these quantities is shown in the case of accreting tori. Figs (6)-*left* combines the information provided by the two functions K_{crit} and ℓ_{crit} together. Using $K=K_{crit}^{\pm}(a;r,\ell)$ and $\ell=\ell_{crit}^{\pm}(a;r)$ in r_{in} and r_{out} of Eq. (14), we obtain functions $\hat{\mathbf{r}}_{\mathbf{in}}^{\pm}(a;r)$ and $\hat{\mathbf{r}}_{\mathbf{out}}^{\pm}(a;r)$ for counterrotating and corotating fluids respectively, providing r_{in}, r_{out} and r_{cent} for each torus, therefore including also the information provided by ℓ_{crit} and K_{crit}. These quantities are essential to determine the **RAD** stability properties, and particularly for the tori collision, and in

[6] We should note also that we use the Boyer-Lindquist frame where $r_+=r_{mbo}^-=r_{mso}^-=r_\gamma^-=M$ at $a=M$ (extreme Kerr **BH**).

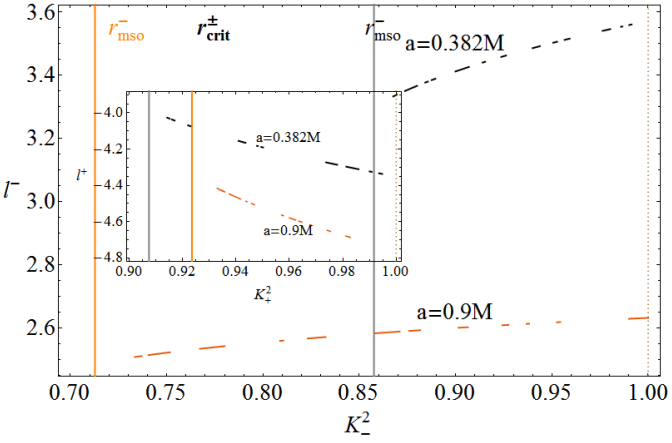

Fig. 10. Fluid angular momentum ℓ versus parameter K^2 for corotating ℓ^- and counterotating fluids ℓ^+ (inset plot), orbiting a **SMBH** with spin $a = 0.382M$ (black line) and $a = 0.9M$ (orange line). Curves of the planes $\ell^{\pm} - K^2$ sets the inner edges of the accreting **RAD** tori. Note that this information is provided by combining ℓ_{crit} and K_{crit} at fixed spin in $r \in]r_{mbo}, r_{mso}]$ with $\ell_{crit} \in]\ell_{mbo}, \ell_{mso}]$ and $K_{crit} \in [K_{mso}, 1[$. Radii $r^{\pm}_{mso}(a)$ for $K^{\pm}_{mso}$, and $K = 1$, correspondent to $r^{\pm}_{mbo}(a)$ are also plotted. Regions bounded by these radii define the tori stability properties and their topology–see discussion in Sec. (2).

the study of the K-modes and ℓ-modes. Increasing the **BH** dimensionless spin, the elongation λ^-, the inner edge r^-_{in} and torus center r^-_{cent} decreases (due to the increasing Lense–Thirring effect). Viceversa, in the counterrotating case, increasing the spin a/M, the (r^+_{in}, r^+_{out}) curves move outwards and the elongation increases, being larger than for the corotating ones (counterrotating tori are generally bigger, with larger equatorial elongation, than the corotating ones). The situation is in fact opposite with the respect to the C$^-$ tori. Furthermore, the larger is the **BH** spin, the greater is the possibility to form a **RAD** with an inner corotating torus (this can be seen for example by comparing the case for **SMBH** with spin $a = 0.7M$ or $a = 0.999M$). The analysis in Figs (6) shows also the limit of small r/M, corresponding to the limiting case of a string of test particle with null elongation. Second panel enlightens further aspect of the symmetry of the ℓcounterrotating couples, by considering the dependence on the central Kerr **BH**, and the functions r_{in} and r_{out} in dependence on K^2 and ℓ. In the study of tori collision emergence, we need to consider this doubled analysis simultaneously. At fixed K^2, increasing a/M and ℓ^+ in magnitude, the tori inner edge r^+_{in} increases, while the outer edge r^+_{out} decreases. Viceversa, for the corotating tori, at fixed K^2, increasing a/M and decreasing ℓ^-, the tori inner edge r^-_{in} decreases, while the outer edge r^-_{out} increases. Curves are bounded by the limiting string particle ring of matter. Increasing K^+, there is an decreases of $\lambda^{\pm}$ (within this special choice of the parameters, a/M and ℓ), while increasing $(|\ell^{\pm}|, a/M)$, the $K^{\pm}$ parameter increases. For a ℓcounterrotating couple, there is in general $r^-_{in} < r^+_{in} < r^+_{out} < r^-_{out}$. The separations of the set of curves increases at large spin, and K^- decreases, giving possible C$^-$ tori all contained in Σ^+_ϵ. From the location of r_{in} it is therefore possible to provide an estimation of the location of r_{out} for accreting tori, and the **BH** spin a/M, with the tori rotation with respect to the attractor. Inner plot confirms the symmetric situation occurring for corotating and counterrotating fluids at fixed K, with different values of the **SMBH** spin. Fig. (10) on the other hand shows the inner edge of accreting tori varying K and ℓ at different **BH** spin a/M. In the corotating case, the difference between the tori inner edge locations, r_{in}, for tori orbiting around **SMBHs** with different spins, is greater then for the counterrotating ones. The corotating fluids are better traces of the **BH** spins. On the other hand, the different behavior with respect to the fluid rotation makes determination of the inner edge of accreting tori a promising method also to eventually distinguish the corotating and counterrotating tori. Figs (11) show surfaces $\ell^{\pm}_{crit}$ =constant in the r/M–a/M plane, each curve sets a special torus. We see different situation for a **BH** spin shift, moving along each curve contained in the possible range of parameter values where accretion onto the central **BH** can occur, considering then locations of the inner edges $r_\times$. Below panels show also the location of the tori centers r_{cent}. The ℓ-modes are confined on a segment bounded by $r = r^{\pm}_{mbo}$ and $r = r^{\pm}_{mso}$ in each strip in the plot, each of them featuring the corotating or counterrotating fluid, on a vertical curve a/M =constant. $K-$-modes are not described by this analysis. A **BH** spin shift corresponds to the translation from a vertical line to another. At fixed spin, the ℓcorotating couples are fixed moving along the curves crossing points, in the same strip, with a fixed vertical line. For the ℓcounterrotating couples, the tori associated with the crossing points of the vertical lines with the curves contained in the two strips have to be considered together. We limited our analysis to the **L1** range of specific angular momentum; we note that for greater magnitude of specific momentum, $\ell \in$ **L2**, the centrifugal component of the force is very high compared with the gravitational one in the force balance, giving rise to the unstable phases of proto-jets configurations. In order to let torus accrete onto the central **BH**, the angular momentum magnitude has to decrease to reach the values of the **L1** range. As already mentioned, we find indications that $()^- < ()^+$ couple, i.e. a couple formed by an external counterrotating and inner corotating torus, are expected to be the favorable ℓcounterrotating couples to be observed. The ℓ-modes are realized as a shift, on a vertical line, form one curve to another on the same strip. A further analysis considers K_{crit} values with a similar approach, this analysis will be also resumed in Sec. (4.3) in the evaluation of the **RAD** tori accretion rates.

4 Emergence of collision

We identify the following three situations where a collision arises: **1.** The $\mathbf{C}_{coll}$ couple with contact in $r^o_{in} = r^i_{out} \equiv r_{coll}$, for (non-accreting or accreting) ℓcorotating or ℓcounterrotating tori. In this colliding couple the outer torus is non-accreting Fig. (1)-right. $\mathbf{C}_{coll}$ eventually leads to tori merging. **2.** The $\mathbf{C}_\times$ couple featured in Fig. (2). This process implies emergence of the outer torus instability. This situation is possible only for the $()^+ \ll_\times$ C$^-_\times$ tori in spacetimes with $a \neq 0$, within the necessary conditions discussed below in Sec. (4.1). The fluid accreting onto the central **BH** necessarily impacts on the (non-accreting or accreting) inner torus. **3.** Finally, the $\mathbf{C}^\times_{coll}$ colliding couple would emerge as a combination of the two processes considered before, this is therefore a $(\mathbf{C}_{coll}, \mathbf{C}_\times)$ combination,

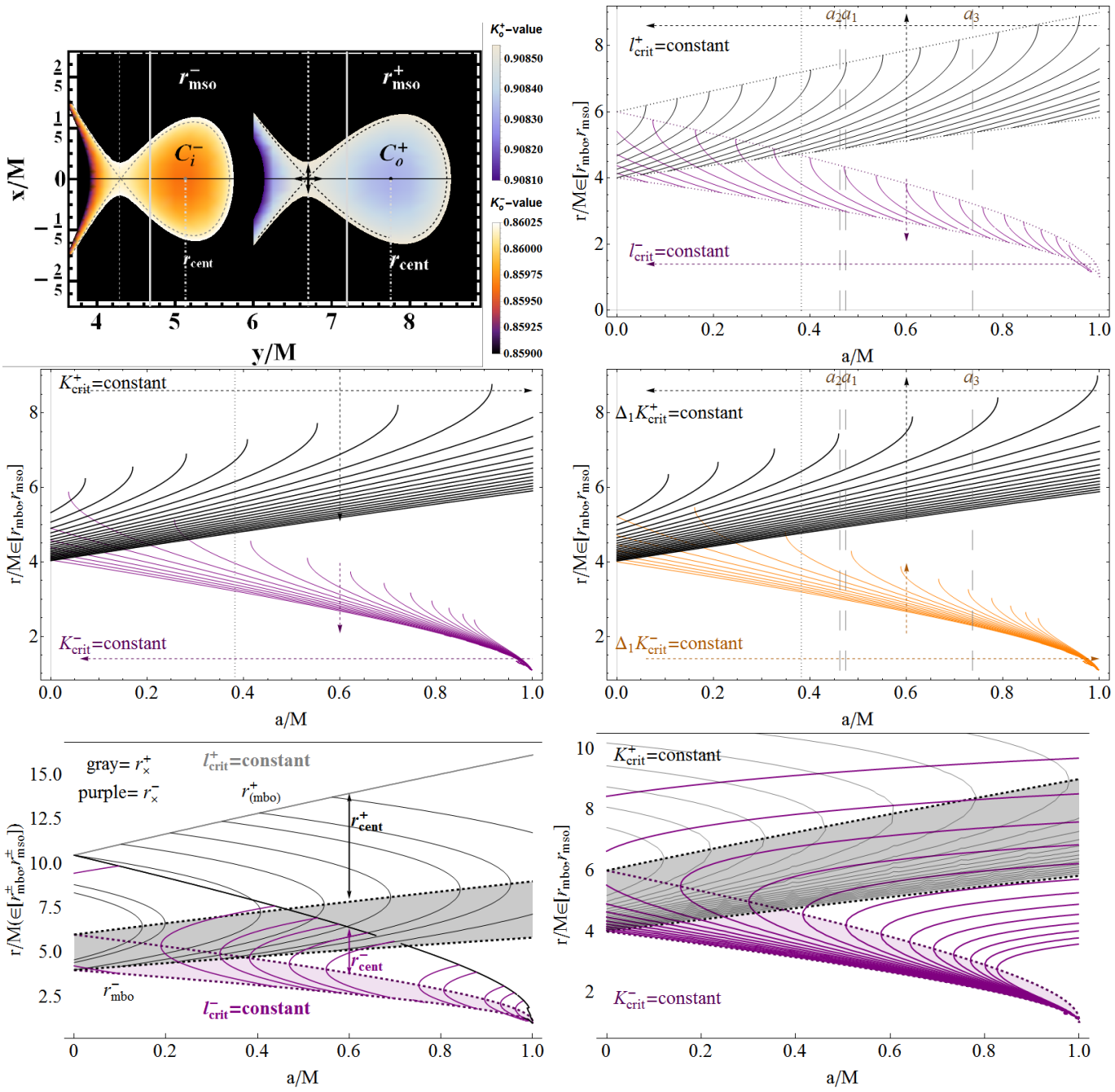

Fig. 11. *Upper left panel*: **GRHD** numerical 2D integration of Eq. (7) for a double toroidal configurations (**RADs** of the order $n = 2$) There is **BH** spin $a = 0.382M$, $\ell^o_+ = -3.99$ and $\ell^i_- = 3.31$, vertical arrows set the thickness $\widehat{\mathbf{h}}^+_s$ of the accreting matter flow–see also analysis in Figs (15). *Upper right panel*: Fluid specific angular momentum $\ell^\pm$ =constant in the plane $r \in [r^\pm_{mbo}, r^\pm_{mso}]$ and $a \in [0, M]$, for corotating (purple curves) and counterrotating fluids (black curves). *Center left panel*:Curves $K^\pm_{crit}$ =costant for $a \in [0, 0.9998M]$ and $r \in [r^\pm_{mbo}, r^\pm_{mso}]$ for corotating (purple curves) and counterrotating (black curves) fluids. *Center right panel*: difference $\Delta_1 K^\pm_{crit} \equiv (K^\pm_{crit}(r^\pm_{mbo}) - K^\pm_{crit})$=constant (maximum location of inner edge is $r_\times \lessapprox r_{mso}$), as function of $a/M \in [0, 0.9998]$ and $r \in [r^\pm_{mbo}, r^\pm_{mso}]$, for corotating (-) (orange), and counterrotating (+) fluids (black). Arrows in the plots follow increasing values of the plotted functions. Spins $(a_1 a_2, a_3)$ are also plotted. Dotted vertical line is $a = 0.382M$. *Bottom panels* show extended plots with indication of the torus centers location (region where $r^\pm_{cent}$ exist are pointed with doubled arrows).

where $r^i_{out} = r^o_\times = r_{coll}$. Collision is combined with an hydro-gravitational destabilization (Paczyński-Wiita mechanism) or any other local instability of the outer torus.

Tori collisions arise due to different causes; in general, $\mathbf{C}_{coll}$ collision occurs when the outer torus grows or loses its angular momentum, approaching the accretion phase. Collisions due to *inner* torus growing is a particularly constrained case. In general, the inner torus evolution affects the $\mathbf{C}_{coll}$ emergence mainly in the early stages towards the accretion; the inner torus instability in several cases would prevent collision. In Sec. (4.1) we discuss the constraints on different couples of tori enabling emergence of collision, and in Sec. (4.2) we provide an evaluation of the center-of-mass energy (E_{CM}) for two colliding particles from the pair of interacting tori.

4.1 Constraints

Emergence of tori collision is featured by several constraints. Here we consider the constraints on the tori angular momentum.

First, the ℓcorotating tori are characterized by the relation $\ell_o/\ell_i > 1$ (this may be verified by drawing the line ℓ =constant for each curve $\ell(r)$ in Fig. (2)). For the ℓcounterrotating tori, the situation is much more complicated; in this case we have to analyze simultaneously the curves $\mp\ell^{\pm}(r)$. The fluid specific angular momentum range of colliding configuration ($\mathbf{C}_{coll}, \mathbf{C}_\times, \mathbf{C}^\times_{coll}$) is constrained by the following relations:

$$\begin{aligned} &\text{for} \quad ()^- < ()^+ \quad \text{there is} \quad |\ell^-/\ell^+| < 1 \\ &\text{and} \quad \ell^- \in]\ell^-_{\rm mso}, \ell^-(r^+_{cent})[. \end{aligned} \tag{17}$$

Also this result can be verified by drawing the line ℓ^- =constant and $-\ell^+$ =constant for each curve $\ell(r)$ in Fig. (2). Relation (17) implies that the angular momentum of matter in the outer counterrotating torus is *always* greater in magnitude than the angular momentum on the inner corotating one.

Furthermore, relation (17) restricts the location of the center r^-_{cent} of the corotating tori of the couple in the following way

$$\begin{aligned} &r^-_{cent} < \bar{r} \quad \text{where} \quad \bar{r} > r^-_{\rm mso}: \quad \ell^- = -\ell^+ > -\ell^+_{\rm mso} \\ &\text{and} \\ &\text{if there is} \quad ()^- = \mathrm{C}^-_\times \quad \text{then} \quad r^-_{cent} \in]r^-_{\rm mso}, r^-_{\rm (mbo)}[. \end{aligned}$$

However, not all the $()^- < ()^+$ couples satisfy the conditions for the outer torus accretion: in many cases an outer torus instability would be preceded by collision and merging with the inner torus.

In fact, the *necessary* (but not sufficient) conditions for the outer torus accretion are provided by the relation $()^- \ll_\times ()^+$, with $-\ell^+_o \in]-\ell^+_{\rm mso}, -\ell^+(r^-_{\rm mso})[$ and $\ell^-_i \in]\ell^-_{\rm mso}, \ell^-(r^+_{\rm mso})[$. It is easy to show that this also implies the remarkable conclusion that there are no more than $n_{\rm max} = 2$ tori satisfying these properties, while any further outer torus (or even a torus internal to the couple) must be non-accreting.

Conversely, particularly for $a \gtrsim 0$, some of these solutions do not allow an outer torus accretion: in fact the accretion takes place only if there is $\ell^- \in]\ell^-(r^+_\times), \ell^-(r^+_{cent})[$, where $()^- \ll_\times \mathrm{C}^+$. On the other hand, then for $()^+ = \mathrm{C}^+$ (i.e. a non-accreting counterrotating tori), there is $\ell^-(r^+_\times) \in]\ell^-_{\rm mso}, \ell^-(r^+_{cent})[$. Particularly, for $\ell^- \in]\ell^-_{\rm mso}, \ell^-(r^+_\times)[$, with $()^- >_\times ()^+$, more then $n_{\rm max} = 2$ tori may satisfy these conditions ($\ell_{o/i} = -1$, $\ell^-/-\ell^+ \gtrsim 1$). Finally the conditions for the $()^+ < ()^-$ couples in $\mathbf{C}_{coll}$ collision are more articulated. We proceed from the analysis of radial $\ell^\pm$ profiles, and the following two cases are possible

$$\begin{aligned} &\textbf{(1)}\ ()^+ \ll_\times \mathrm{C}^-, \ (a \gtrsim 0) \quad \text{where there is} \quad n_{\rm max} = 2, \\ &\quad \text{and} \\ &\textbf{(2)}\ ()^+ < \mathrm{C}^-, \quad \text{with} \quad ()^+ >_\times \mathrm{C}^-. \end{aligned}$$

The first case-(**1**) then implies the maximum number of tori $n_{\rm max} = 2$.

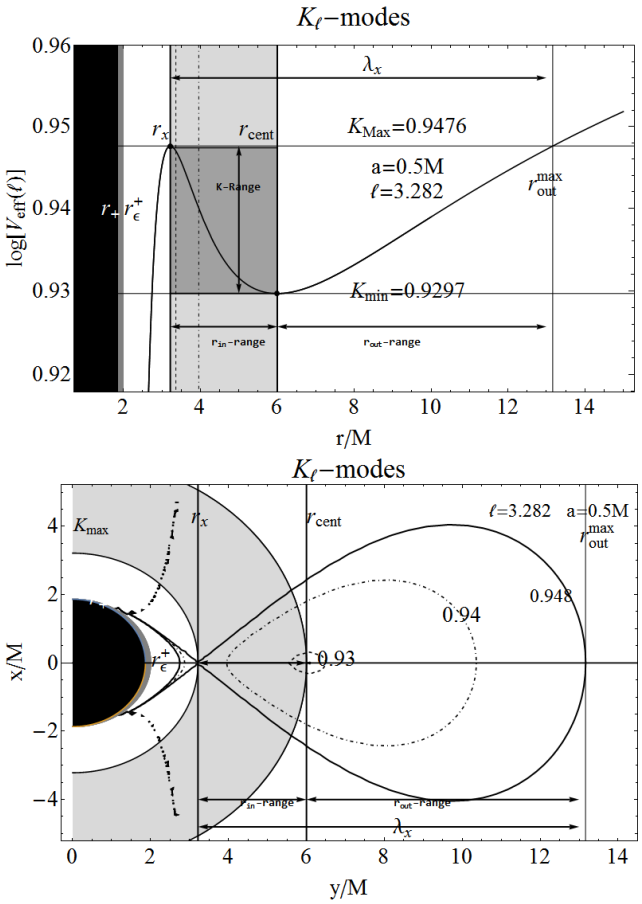

Fig. 12. Illustration of K_ℓ-modes. *Upper panel* shows the function $W_{\bar{\ell}} = \ln[V_{eff}(\ell)]|_{\bar{\ell}}$, in Eq. (7), at constant angular momentum $\bar{\ell}$. The effects of modes, $K_\ell \in [K_{min}, K_{\rm max}]$ are illustrated by the range of parameters and variables variations (shaded-labeled regions): K-range (dark gray), inner torus edge r_{in}-range (light-gray), outer torus margin r_{out}-range (white). Arrows indicate the ranges. The torus maximum elongation $\lambda_\times$, following the K_ℓ-modes is also shown. r_{cent} is the maximum pressure point of the torus, r^+_ϵ is the outer ergosurface, black region marks the range $r \le r_+$ where r_+ the the outer **BH** horizon. In the **RAD** context, the study of K_ℓ-modes for one torus, must be coupled with the K_ℓ-modes for any other component of the aggregates and with the ℓ-modes–Fig. (13). *Bottom panel*: Some torus profiles corresponding to different values of K. Light-gray circular region corresponds to the r_{in}-range.–See also Figs (5).

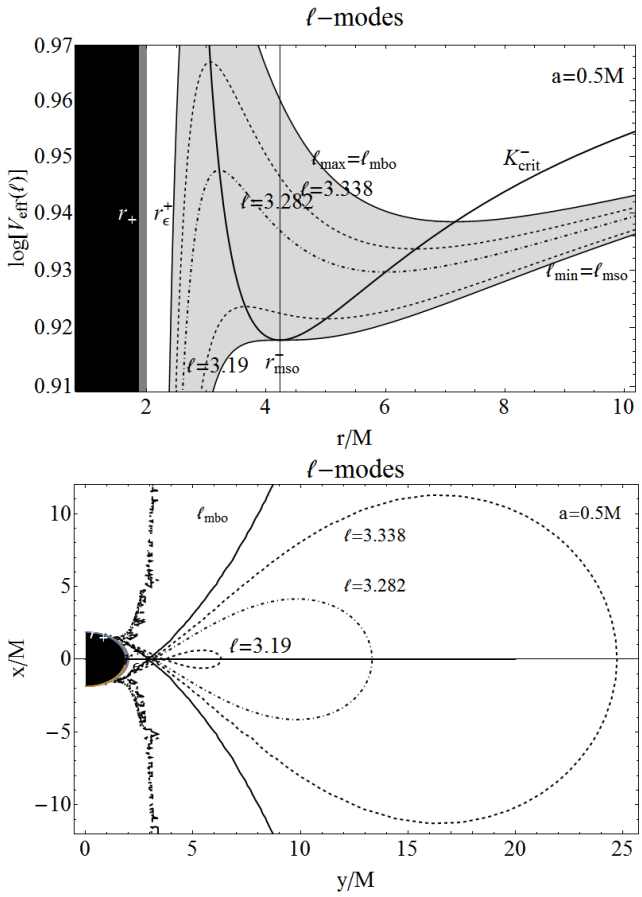

Fig. 13. Illustration of ℓ-modes. *Upper panel*- The function $W = \ln[V_{eff}(\ell)]$, in Eq. (7), for different values of the fluid specific angular momentum ℓ. ℓ-range, maximum range of variation of the ℓ parameter, $\ell \in [\ell_{mso}, \ell_{mbo}[\equiv [\ell_{\rm min}, \ell_{\rm sup}[$, is light-gray colored. Black-thick curve marks K_{crit} for the fixed value **BH** dimensionless spin a/M–see also Fig. (5). *Bottom panel*-torus profiles, corresponding to different values of $\ell \in \ell$-range. r_ϵ^+ is the outer ergosurface, black region marks the range $r \leq r_+$ where r_+ is the outer **BH** horizon. The analysis of ℓ-modes of each torus of the **RAD** must be combined with K-modes ℓ-modes for any other **RAD** component; ℓ-modes are associated to shifts related points on the K_{crit} curve (at fixed a/M) (each point sets a different minimum and maximum pressure point, each point of the such a couple on K_{crit} sets different angular momenta. On the other hand only for accreting tori, curves K_{crit} =constant fix $r_\times$ and r_{out} of the accreting torus correspondent to one fixed value of specific angular momentum-see also Figs (5) and Figs (8,9,6,10,11).

Then, if we define the radius $\bar{r}^-$: $\ell^-(\bar{r}^-) = -\ell^+$, then there are the two possibilities for (**1**) and (**2**):

$$\text{–there is} \quad |\ell^-/\ell^+| > 1 \quad if \quad r^-_{cent} > \bar{r}^- \tag{18}$$

which implies case (**b**) $n_{\rm max} \geq 2$. Or

$$\text{– there is} \quad |\ell^-/\ell^+| < 1 \quad if \quad r^-_{cent} \in]r^+_{cent}, \bar{r}^-[. \tag{19}$$

In various aspects of this work it was stressed that we adopted a constraints analysis, through the use of quantities defined in Eqs (12), choosing a family of parameters $\{\mathbf{p^i}, \mathbf{p^o}, a/M\}$ for the description of the **RAD** orbiting around a **SMBH** with dimensionless spin a/M. For a wide discussion on the application of this method in the collision emergence we refer to the [29], while here we point out that tori collision is essentially determined, at *fixed* value of the specific angular momentum, (ℓ_i, ℓ_o) and of the **SMBH** parameter a/M, by the **RAD** K_ℓ-modes featuring, for increasing values of K, the torus growth and the increase of torus elongation λ on the equatorial plane–this quantity pictured in Fig. (7) and considered also in Fig. (8) in given explicitly in Sec. (3). The K- and ℓ and K_ℓ-modes are some of the modes for **RAD** associated with the various perturbative approaches explored in [27], here we do not go into the details of this issue, being beyond the purpose of the present work, but we limit ourselves to the description of some modes adapting the discussion to the purposes faced here. First, the perturbations arising in the ringed disk structure are generally meant to be perturbations of its toroidal components, subjected to different constraints and generated by perturbing the **RAD** effective potentials in Eq. (12) or, equivalently, perturbations of the sequences of parameters $\mathbf{p} = \{\mathbf{p}_i\}_{i=1}^n$. There are several sub–modes associated with two main mode classes ℓ- and K modes. Keeping the other parameters fixed, we could speak of *K-mode* or *ℓ-mode* of the perturbation respectively. The **RAD** can be perturbed in one of these modes or in a combination of them, and each mode can have some sub-modes defined by the restrictions on the perturbation, bounded by specific relationships on the spacings and elongations. Keeping the sequence of parameters $\{\ell_i\}_{i=1}^n$ fixed, the perturbations will be only on the Heaviside functions in the effective potential (12). This is a one dimensional problem (actually this is entirely fixed by the radial direction only, thought the **RAD** is generally a "knobby" accretion disk–see discussion in Sec. (3)). If each ℓ_i is fixed, then the range of variation for K is comprised in a limited ranged defined by the value of ℓ_i. It should be noted that this kind of perturbation is actually a (rigid) perturbation of the inner and outer edges of each torus (or also the elongations λ_i at fixed center r^i_{cent}): i.e., the perturbation of an edge is transmitted rigidly to the other range, with fixed center r_{cent}. The elongation λ_i is however not conserved (when this is imposed one has the $K_\lambda-$modes). The $K-$modes may lead effectively from a quiescent torus with angular momentum in the range **L1** to an accreting phase or, viceversa, to block the accretion (for example this may occur in the so called "drying–feeding"-processes considered in [29]). Nevertheless both these modes preserve the symmetry for reflection on the equatorial plane of the **RAD**, but the perturbation generally leads also to a change in the vertical direction with a change of the height h_i in each subconfiguration–see also Fig. (7). Varying ℓ_i at fixed K_i, the Boyer surfaces are not rigidly translated (a shift in the torus center r^i_{cent}) on the radial direction, but the torus morphology and, in particular, its thickness changes. In the ℓ-modes an increase in the specific angular momentum magnitude means a perturbation outwards of the torus center (which viceversa is kept fixed by K-modes), leading to a radial movement outwards. The ℓ-modes can also lead (even at fixed K) to a change of the tori equilibrium from a quiescent phase to the accretion onto the central **SMBH** with the decrease of specific angular momentum magnitude. As seen in Figs (5,12) and (13), K-parameter varies in the range $[K_{\rm min}, K_{\rm lim}[$, i.e., K is bounded from below by the limiting case of test particle ring with zero pressure contribution and from above by the limit $K_{\rm lim}$, i.e. $K_{\rm max}$ correspon-

dent to the point of minimum pressure, or $K_{\rm lim}=1$, depending on the angular momentum in **L1** or (**L2**, **L3**) respectively. Actually, for the **j**-torus of the aggregate, $K^{\mathbf{j}}_{\rm lim}$ is bounded by the presence of the adjacent tori [27]–see also Eqs (12). ℓ-modes are considered in Figs (5) and Figs (13), while $K-$modes are in Fig. (12). A significant part of this investigation accurately evaluates the totality of these possibilities for ℓcorotanting and the ℓcounterrotating cases complectly describing the model – Fig. (8,9,6,10).

4.2 Center-of-mass (CM) energy

We can now evaluate CM energy ($\mathrm{E_{CM}}$) for two colliding particles from the tori in $\mathbf{C}_{coll}$, $\mathbf{C}_{\times}$ or $\mathbf{C}^{\times}_{coll}$ couples, in the test particle approximation, with four-momenta p^a_j and rest masses μ_j. There is:

$$\begin{aligned}&\mathrm{E}^2_{\rm CM}=-p^a_{tot}p_{tot\,a}=\mu_i^2+\mu_o^2-2g_{ab}p^a_i p^b_o,\\&\text{where}\quad p_{tot}\equiv p_i+p_o,\end{aligned}\tag{20}$$

as observed by a local observer which is at rest in the CM frame of the two particles.

We consider the cases with at least one circularly orbiting particle (equatorial motion), see [91,92,93,94,95,96]. Then Eq. (20) reads

$$\begin{aligned}&\mathrm{E}^2_{\rm CM}=\frac{2p^\pi_t[r^3+a^2[2-2\overline{\ell}_T+(2-r)\overline{\ell}_\pi+r]]}{r(r^2-2r+a^2)}+2\mu^2,\\&\text{where}\quad \overline{\ell}_T\equiv\overline{\ell}_i+\overline{\ell}_o,\quad \overline{\ell}_\pi\equiv\overline{\ell}_i\overline{\ell}_o,\quad p^\pi_t\equiv p^i_t p^o_t\end{aligned}\tag{21}$$

($M=1$, $\mu_i=\mu_o\equiv\mu$). We note that $\mathrm{E}^2_{\rm CM}$ in Eq. (21) is function of the ratio $\overline{\ell}_i\equiv\ell_i/a$ (for $a>0$) [26] within Eqs (17,18). Whereas the dependence on the torus masses and elongations on the equatorial plane derives from p^π_t related to the contact point r through, at least, p^i_t. By considering the test free particle limit we use the definition of ℓ with p_ϕ and p_t constant–see also discussion in Sec. (4.3).

The contact (collision) point r in Eq. (21) is r_{coll} for the case $\mathbf{C}_{coll}$, where there is $u^i_r(r_{coll})=u^o_r(r_{coll})=0$ (u_r is the radial velocity), it is r^i_{out} for the case $\mathbf{C}_\times$ (where there is $u^i_r(r^i_{out})=0$), and it is $r^\times_{coll}=r^i_{out}=r^o_\times$ (with $u^i_r(r^\times_{coll})=u^o_r(r^\times_{coll})=0$) for $\mathbf{C}^\times_{coll}$.

Note that in these three cases, there is always $u^i_r=0$ (circular motion assumption). For ($\mathbf{C}_\times$, $\mathbf{C}^\times_{coll}$) (with $()^-\ll_\times \mathrm{C}^+_\times$), there is $r=r_\times$ and fluid specific angular momentum $\ell_o=\ell^+(r^o_\times)$, $\ell_i=\ell^-(r^i_{cent})$.

We consider the energy $\mathrm{E_{CM}}$ for a free falling particle approximation from $r^+_\times=r^+_{\rm mso}$ on a thin ring of matter close to $r^-_{\rm mso}$ (i.e. $\mp\ell_\pm\gtrsim\mp\ell^\pm_{\rm mso}$, and $r^+_{cent}=r^+_{\rm mso}$), reducing formally to the problem of "on-ISCO" collision from an "in-ISCO" particle considered in [91,95,97].

However, even within the test particle approximation, in the cases $\mathbf{C}_\times$, $\mathbf{C}_{coll}$ and $\mathbf{C}^\times_{coll}$, we retain the constraints on $(\overline{\ell}_T,\overline{\ell}_\pi)$ in $\mathrm{E}^2_{\rm CM}$ for the torus formation and emergence of collisions–see also Table (1) for a summary of the notation introduced in this section.

In general, for a $\mathbf{C}_\times$ collision in a couple $()^-<\mathrm{C}^+_\times$ (with outer counterrotating torus in accretion and inner corotating quiescent or in accretion onto the central **BH**), we use the assumption of a free particle at $r_\times$ and p^o_ϕ =constant. In this tori couple inner torus acts as a "screening" torus for the outer accreting torus. For the inner torus, the situation is much more complex and we could not use the free particle approximation except in the case of an inner thin ring of matter. Leaving the treatment of the general situation for future analysis, in Fig. (14) we restrict our consideration to some simple assumptions: in the $\mathbf{C}_{coll}$ case, we evaluate $\mathrm{E_{CM}}$ for two circularly orbiting particles with constants $(-p_t,p_\phi)$ at r_{coll}. This situation may be applied for ℓcorotating and ℓcounterrotating cases, eventually we could consider the inner torus in accretion.

Then, a particularly interesting situation occurs when the inner torus of $\mathbf{C}_{coll}$ is accreting, or the outer torus of $\mathbf{C}^\times_{coll}$ is in accretion or finally, the two tori are accreting in a $()^-<<_\times \mathrm{C}^+_\times$ couple. Within the assumption of circular motion in r_{coll} for the outer torus, there is $\ell^o>p^o_\phi(r_{coll})$ in magnitude, while for the inner torus the situation is more complicated. By solving the hydrodynamic equations (6) for each torus, with $r^o_{in}\geq r^i_{out}$, it is possible to find that for $()^-<<_\times \mathrm{C}^+_\times$, see Table (1), the points $(r^+_\times,r^\times_{coll})$ are in the range $]r^+_{\rm mbo},r^+_{\rm mso}]$ only for $a\in[a_0,M]$, where $a_0\equiv 0.372583M$–Fig. (2) and Figs (3) for a_0. This means that collision with an outer counterrotating accreting torus can occur in these geometries *only*. In fact: this can be also seen, by noting that a $()^+_{\rm I}$ configuration (with $\mp\ell^\pm\in]\mp\ell^\pm_{\rm mso},\mp\ell^\pm_{\rm mbo}[$) cannot cross the orbit $r^-_{\rm mso}$ ($r^-_{\rm mso}\notin()^+_{\rm I}$) for $a>a_0$, while for $a<a_0$ there is $r^-_{\rm mso}\in\mathrm{C}^+_\times$, and $r^-_{\rm mso}\in\mathrm{C}^+$, if $\ell^+\in[-\ell^+(r^-_{\rm mso}),-\ell^+_{\rm mbo}]$.

Crossing of $(r^+_{\rm mso},r^+_{\rm mbo})$ in $()^-_i$ assures that the $\mathrm{E_{CM}}$ evaluation in Fig. (14) is well grounded. Figure (14) shows evaluations of the energy $\mathrm{E_{CM}}$ for different coupled of tori in dependence on the **BH** spin a/M.

A rapid look at Figure (14) reveals that for the collisions $\mathbf{C}_\times$, the energy center-of-mass energy $\mathrm{E_{CM}}$ can be arbitrarily large due to increasing **BH** dimensionless spin up to $a=M$.

4.3 Evidences of double accretions

From observational view-point a relevant aspect of the **BHs** astrophysics related to the interaction of central **BH** with the **RADs** consists in the possibility that a **RAD** would have been indeed observed so far and identified as the case of one accretion torus orbiting its central **BH** attractor: this possibility, also discussed in [30], challenges the description of **RAD** as an whole orbiting toroidal structure despite its internal complex dynamics. In order to do this in [27], the definitions of **RAD** elongation and thickness, and the **RAD** distribution of angular momentum were provided, while in [30] these systems were carefully related to the characteristics of the **SMBHs** attractors. This new framework can be particularly interesting and can have important implications in the processes analyzed in [98,99,100,101,102,103,104], where the hypothesis of different accretion stages are claimed as ground to justify the **SMBH** masses at high redshift, and can have a relevant role in the studies of the X-ray screening emission where an accreting torus is supposed to be adjacent to an obscuring torus (i.e. a $()^-<\mathrm{C}^+_\times$ couple, or a combination of these in the **RAD** model). However, our analysis strongly constrains this possibility. Different accreting phases may be explained in the **RAD** model

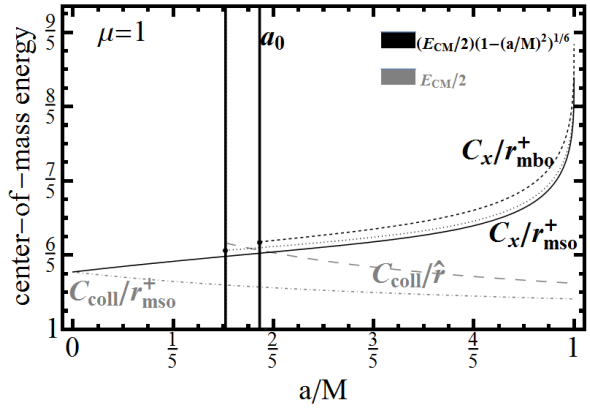

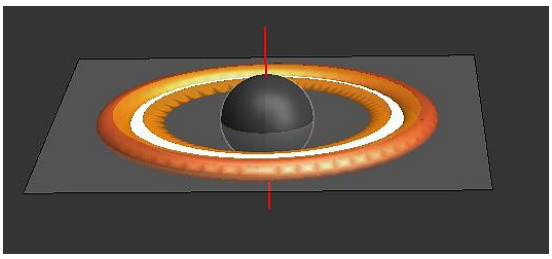

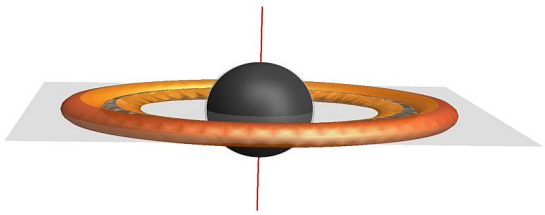

Fig. 14. *Upper* panel: Center-of-mass energy $E_{CM}/2$ in the test particle approximation, versus a/M, for the couples $()^- <<_\times C^+_\times$–Figs (2) and Figs (1). We consider: infalling particle from r^+_{mso} black curve (r^+_{mbo}-dashed-black curve) of $\mathbf{C}_\times$ colliding configuration. They are labeled respectively as $\mathbf{C}_\times/r^+_{mso}$ (black curve) and $\mathbf{C}_\times/r^+_{mbo}$ (dashed-black curve)). Dotted black curve is for a particle from orbit $\hat{r} \equiv r^+_{mso} - 2M$ colliding on a circular orbiting particle located at r^-_{mso}-(for the asymptote-factor $(1-(a/M)^2)^{1/6}$). Collision of counterrotating particles on an inner corotating thin ring at r^+_{mso} ($\hat{r}$) are indicated with $\mathbf{C}_{coll}/r^+_{mso}$(dotted-dashed gray curve) and $\mathbf{C}_{coll}/\hat{r}$ (dashed gray curve) respectively, -see also [91]. Main notation is also listed in Table (1). *Center panel:* **GRHD**-numerical 3D integration of Eq. (7) proving the density surfaces of colliding ℓcorotating $C^-_i < C^-_o$ couple of corotating ($\mathbf{C}_{coll}$) tori, with specific angular momentum $\ell^-_i = 3.3$ and $\ell^-_o = 3.4$ and K parameter ($K^-_i = 0.927$, $K^-_o = 0.935$) respectively. Black region is $r < r_+$, r_+ is the outer horizon of the black hole of spin $a = 0.385M$, gray region is the outer ergosurface, color are chosen according to improved visual effect, integration is stopped at the emerging of tori collision–see also Fig. (1). *Bottom panel*, different view of the colliding couple $\mathbf{C}_{coll}$ to enlighten the colliding region. Tori are coplanar and centered on the central **BH** orbiting on its equatorial plane.

for example by a simultaneous accretion phases in the couples $C^-_\times < C^+_\times$, or a discontinuous accreting phase induced by the internal **RAD** evolution (for example a "drying-feeding" effect described in [29] and considered in Sec. (4.2)). Our analysis shows how the **RAD** formation is actually highly constrained and strongly limited by several factors, such as its angular momentum distribution, particularly by the dimensionless spin of the central attractor, rendering the contexts where to potentially observe these objects sharply focused and precise [29,30,32]. Moreover, the possible inter-disk activity in the agglomerate, such as the arising of proto-jets [32,28], collision or double accretion here analyzed in details, shows a quite large template of phenomenology associated to the **RAD**.

It is then important to note that in general the **RAD** is in fact a "knobby" accretion disk; in the $n = 2$ case, the K and ℓ modes and the evolution of each **RAD** component is determined by a variation of the distribution of the matter in the **RAD**. Note that an ℓcounterrotating *accreting* couple has no special constraints on the relative height of the tori. This obviously implies a very wide set of possibilities for a knobby **RAD** disk. First, as demonstrated in [27], a **RAD** is always a geometrically thin accretion disk. In order to fix some ideas we provide here some specific considerations for a $C^-_\times < C^+_\times$ couples of Figs (11). We can easy evaluate many of the **RAD** characteristics, as the **RAD** thickness (h) and elongations (λ), tori spacings ($\bar{\lambda}_{i,o}$) showed in Fig. (7), through an assessment of the K-parameter only–for a precise definition and discussion on this quantities we refer to [27]. We focus in particular on the case of Fig. (2) and Fig. (11) where there is $a = 0.382M$, $\ell^+_o = -3.99$ and $\ell^-_i = 3.31$. In this specific case, the **RAD** aggregates a set of rather small tori. In fact: for the counterrotating torus, $C^+_\times$, there is $r^+_{cent} = 7.75994M$, $r^+_\times = 6.70523M$, $r^+_{out} = 8.4422M$, with elongation $\lambda^+ = 1.73696M$, while the torus height is $h^+/2 = 0.223684M$; for the corotating torus, $C^-_\times$, the torus center, the inner and outer edges are located at $r^-_{cent} = 5.13459M$, $r^-_\times = 4.28942M$, $r^-_{out} = 5.73609M$, while the torus elongation is $\lambda^- = 1.44667M$, and the high $h^-/2 = 0.230375M$. The spacing $\bar{\lambda}_{i,o}$ between two consecutive tori regulates the collision, the **RAD**-modes, its formation and in the analysis of the stratified **RAD** X-ray emission spectra, and can determine the effects of the X-ray screening. In fact, in the couple $C^-_\times < C^+_\times$, we also recall that screening effects are only possible with the corotating tori as follows $C^-_\times < C^- < ... < C^+_\times < C^\pm$. The inner accreting corotating torus may act as a screening torus for the accreting outer counterrotating torus together with any inner, quiescent corotating torus, formed in the spacing region. It is therefore clear that this situation may occur only in the first phases of evolution for the outer torus, depending on the spacing in the tori couple. The spacing for the special $C^-_\times < C^+_\times$ couple of Fig. 2 is $\bar{\lambda} \equiv r^o_\times - r^i_{out} = 0.969137M$. Note that the space-scales are in units of **SMBH** masses (i.e. $10^6 M_\odot$–$10^9 M_\odot$– $M_\odot$ being solar mass)– [27]. Such a couple can be observable orbiting any Kerr **BH**, and the larger is the **BH** dimensionless spin, the bigger the tori can grow, while a larger spacing is required. In fact, an immediate evaluation shows that the maximum spacing possible for a double accreting couple is $\bar{\lambda}_{max} \lesssim 8M$, in the case of a near extreme Kerr **BH** where $a \approx M$. This also shows how **SMBHs**and high spin **BHs** are the most promising attractors for **RAD** formation and particu-

larly for the most articulated structures as the ℓcounterrotating tori, with a double accretion or screening tori.

Below we provide an investigation of mass accreting rate, related to **RAD** tori, and other significant functions of the accreting disks physics focusing on their dependence on the **SMBH** spin, and the differences between corotating and counterrotating fluids.

4.4 Tori from polytropic fluids

We consider **RAD** tori with polytropic fluids: $p = \kappa\varrho^{1+1/n}$ (here n should not be confused with the **RAD** order). In Sec. (4.4.1) we shall discuss this hypothesis more closely with some additional considerations, here we note that this hypothesis allows us to provide estimates of different quantities of each torus, which are extremely important for the evaluation of the energy release from **RADs**. In particular the mass-flux, enthalpy-flux (evaluating also the temperature parameter), and the flux thickness–see [52] and [105]. In details, these quantities are listed in Table (2). We note that each of these quantities can be express in the general form $\mathcal{O}(r_\times, r_s, n)$ of Table (2), where $q(n,\kappa)$ and $d(n)$ are different functions of the polytropic index $\gamma = 1 + 1/n$ and polytropic constant κ or as $\mathcal{P}$ form, for example the mass flow rate through the cusp (mass loss, accretion rates) $\dot{M}_\times$, and the cusp luminosity $\mathcal{L}_\times$ (and the accretion efficiency η), measuring the rate of the thermal-energy carried at the cusp. The relativistic frequency Ω reduces to Keplerian values Ω_K at the edges of the accretion torus, where the pressure forces are vanishing (The limiting case of polytropic index $\gamma = 0$ would correspond to the case of zero pressure represented by the dust of test particles)). Note that this also justifies the approximations for collision energy evaluation of Fig. (14). Parameters (κ, n) within the constraints $q(n,\kappa) = \bar{q}$ =constant, fix a polytropic-family. The $\mathcal{O}(r_\times, r_s, n)$ depends on the location of the inner edge of the accreting torus, constant for K-modes, but variable with the **RAD** ℓ-modes, and on theradius r_s which is the related to the thickness, $\overleftarrow{\mathbf{h}}_s$, of the matter flow[7] (see also Fig. (11)). Then, as the cusp approaches the limiting radius r_{mbo}, the potential $W_\times \approx 0$, which is also the limiting asymptotic value for very large r as well as for the emergence of the proto-jets for $\ell \in$ **L2**.

$\mathcal{P}$- and $\mathcal{O}$-quantities of Table (2) are evaluated for corotating and counterrotating tori in Figs (15), for dimensionless **SMBH** spin $a/M \in [0,1]$. To simplify our discussion, we have considered for the analysis of the two classes of the functions the following reduced quantities:

$$\textbf{[}\mathcal{O}\textbf{-quantities]}\text{:}\mathcal{R}^\pm_* \equiv (W^\pm(r_s) - W^\pm_*)^\varpi \quad \text{and } (W^\pm(r_{mbo}) - W^\pm(r_{mso})) \tag{22}$$

$$\textbf{[}\mathcal{P}\textbf{-quantities]}\text{: } \mathcal{N}^\pm_* \equiv \frac{r_*(W^\pm(r_s) - W^\pm_*)^\varpi}{\Omega_K(r^\pm_*)} \quad \text{where} \quad r_s = r_s(a) \in]r_\times(a), 1[, \tag{23}$$

serving as an immediate and simple way to understand the trends of these functions of the **BH** spin, the fluid angular momentum and the cusp location. In fact, this analysis is especially focused on the characterization of the $\mathcal{P}$- and $\mathcal{O}$-quantities for an accreting couple $\mathrm{C}^-_\times < \mathrm{C}^+_\times$, as functions of **SMBH** dimensionless spin a/M, at different locations of the inner edges, $r_* = r^\pm_\times$ and the radius r_s, which is related to the thickness $\overleftarrow{\mathbf{h}}_s$ of the accreting matter flow as in Figure (11). Then $\varpi = n + 1$, with $\gamma = 1/n + 1$ being the polytropic index. Ω_K is the Keplerian angular velocity, where Ω^+_K has been considered for the counterrotating fluids. The maximum location of the accreting torus the inner edge is $r_\times \lessapprox r_{mso}$. Note that in Eq. (22)the maximum difference $(W^\pm(r_{mbo}) - W^\pm(r_{mso}))$ is provided in relation to the analysis of the $\mathcal{O}$ and $\mathcal{R}$ quantities, this function of the a/M is also plotted in Figs (15). This difference clearly features the limiting case where $r_s \lessapprox 1$ and $r_\times \gtrapprox r_{mso}$, providing the maximum (limiting) distance $r_\times - r_s$, and the limiting maximum flow thickness $\overleftarrow{\mathbf{h}}_s$ case. On the other hand, Figs (11) show also lines $(\exp[W^\pm(r_{mbo})] - \exp[W^\pm(r_\times)])$ =constant for different values of **SMBH** spin $a \in [0, M]$ and the inner edge of accreting torus $r_\times \in]r_{mbo}, r_{mso}[$. Note that $\exp[W] = K$. The couple of parameters $\{r_s(a), r_\times(a)\}$ in Eq. (23) has been fixed in the examples of Figs (15), to simplify the comparison of the $\mathcal{O}^\pm$ and $\mathcal{P}^\pm$ quantities in the corotating and counterrotating tori, and to characterize the dependence of these quantities on the **SMBH** spin-to mass ratio a/M. In fact, within this choice, all the quantities $\mathcal{O}$ and $\mathcal{P}$ or, equivalently, $\mathcal{N}$ and $\mathcal{R}$ of Eq. (23), become functions of the spin a/M only; on the other hand, at fixed a/M, we compare these quantities for different radii r_s and $r_\times$, related by fixed relations through the different laws $r_s(a)$ and $r_\times(a)$, as expressed in Figs (15).

It is clear that the $\mathcal{O}$ and $\mathcal{P}$ quantities have similar dependence on the triplet of parameters $\mathbf{p}^{(3)}_F \equiv (a/M; r_*, r_s)$. We consider then the doublet $\mathbf{p}^{(2)^\pm}_F \equiv (r^\pm_*, r^\pm_s)$. There is always $\partial_{a^*} G^\pm|_{\mathbf{p}^{(2)^\pm}_F} \lessapprox 0$ respectively for counterrotating and corotating tori, and $G^+(a)|_{p^{(2)^+}_F} \leq G^-(a)|_{\mathbf{p}^{(2)^-}_F}$, where $G^\pm \in \{Q^\pm, \mathcal{P}^\pm\}$, and $G^+ = G^-$ for $a = 0$ only; here $a^* \equiv a/M$. On the other hand, the spread between corotating and counterrotating curves increases with the **BH** spin, i.e., $\partial_{a^*}(G^-|_{\mathbf{p}^{(2)^-}_F} - G^+|_{\mathbf{p}^{(2)^+}_F}) > 0$. Note that we adopted the parameters $\mathbf{p}^{(2)^+}_F \equiv (r^+_*, r^+_s)$ and $\mathbf{p}^{(2)^-}_F \equiv (r^-_*, r^-_s)$ at fixed a/M, this means that we are comparing ℓcounterrotating tori related through these parameters as indicated in Figs (15). Interestingly then, there is in general $\partial_{a^*}(G^-|_{\bar{\mathbf{p}}^{(2)^-}_F} - G^-|_{\breve{\mathbf{p}}^{(2)^-}_F}) < 0$, where $G^-|_{\bar{\mathbf{p}}^{(2)^-}_F} \geq G^-|_{\breve{\mathbf{p}}^{(2)^-}_F}$, while $G^-|_{\bar{\mathbf{p}}^{(2)^-}_F} = G^-|_{\breve{\mathbf{p}}^{(2)^-}_F}$, asymptotically for $a = M$, and $(\bar{\mathbf{p}}^{(2)^\pm}_F, \breve{\mathbf{p}}^{(2)^\pm}_F)$ are two general couples of parameter, therefore associated to two different curves in Figs (15). As $(\bar{\mathbf{p}}^{(2)^-}_F, \breve{\mathbf{p}}^{(2)^-}_F)$ are functions of a/M themselves as shown in Figs (15), this result may be interpreted as the com-

[7] Note that in some sense this quantity is still dependent on a generalized definition of K-parameter. It is worth specifying here this aspect, as it is also briefly mentioned in Sec. (4.2): if $\ell \in$ **L1** then $K \in [K_{\min}, K_{\max}]$, where $K_{\min} > K_{mso}$ and $K_{\max} < 1$. $K_{\max}$ corresponds to the accreting point $r_\times$, while r_s is directly associated to the accreting flux thickness. Clearly r_s can be write in terms of a K parameter value $K_s \in [K_{\max}, 1[$–Figs (15).

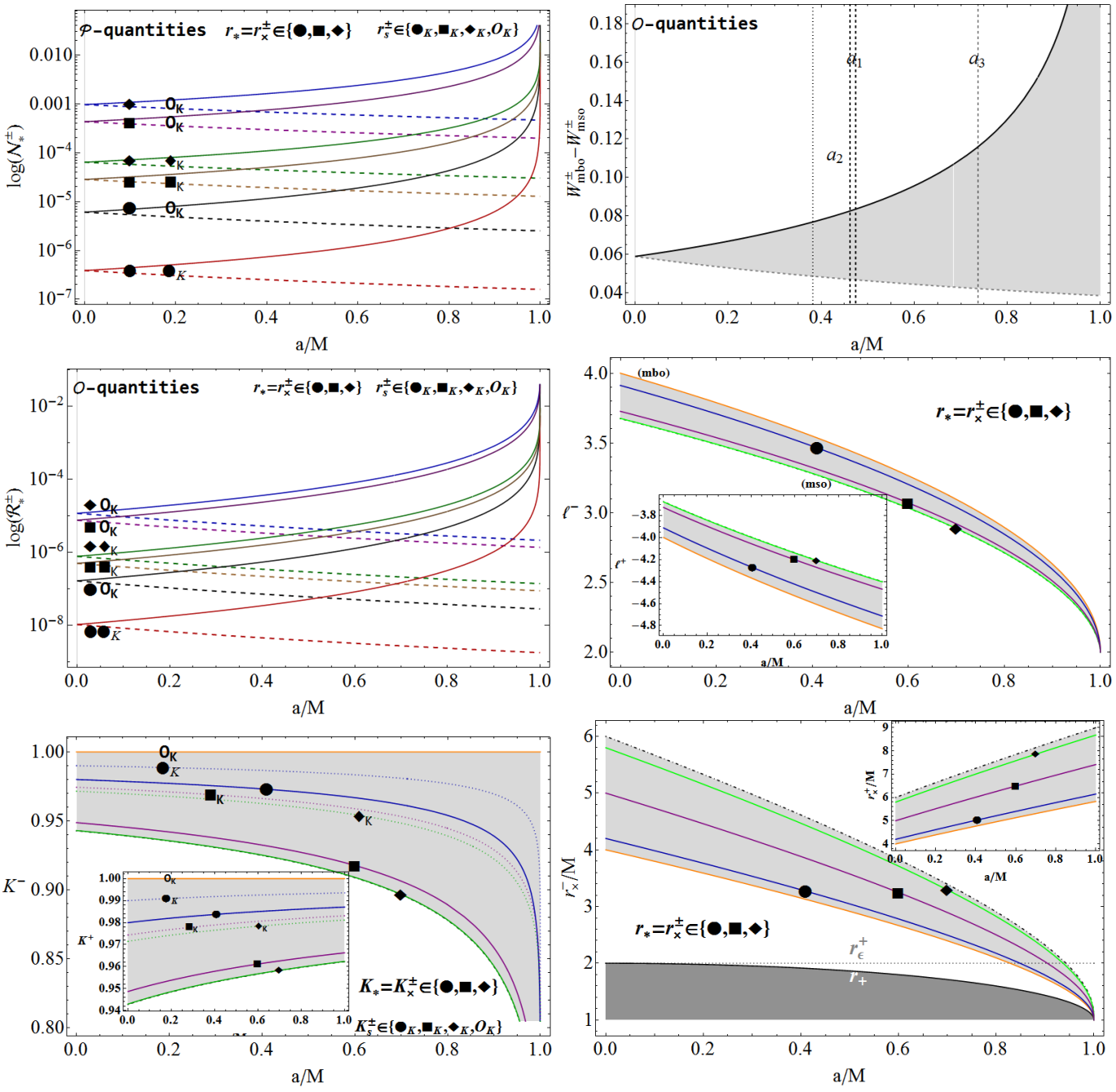

Fig. 15. Evaluation of $\mathcal{P}$- and O-quantities of Table (2) for corotating and counterrotating tori, versus Black hole dimensionless spin a/M. Plots of $\mathcal{N}_*^\pm \equiv r_*(W^\pm(r_s) - W_*^\pm)^\kappa(\Omega_K(r_*^\pm))^{-1}$ (*upper left panel*) for $\mathcal{P}$-quantities analysis; the maximum difference $(W^\pm(r_{mbo}) - W^\pm(r_{mso}))$ (*upper right panel*) (Eqs (22,23)) and $\mathcal{R}_*^\pm \equiv (W^\pm(r_s) - W_*^\pm)^\kappa$ (*center left panel*), for O-quantities analysis as functions of **SMBH** dimensionless spin a/M, for corotating ([-]–continuum curves) and counterrotating ([+]–dashed curves) tori at different $r_* = r_\times^\pm \in \{\bullet, \blacksquare, \blacklozenge\}$ and $r_s \in \{\bullet_K, \blacksquare_K, \blacklozenge_K, \mathrm{O_K}\}$ where $\varpi = n + 1$, with $\gamma = 1/n + 1$ is the polytropic index. Radii (r_*, r_s) and the correspondent angular momentum ℓ and K parameters are shown with $\{\bullet, \blacksquare, \blacklozenge, \bullet_K, \blacksquare_K, \blacklozenge_K, \mathrm{O_K}\}$. Ω_K is the Keplerian angular velocity, $r_\times$ is the accreting tori cusp (inner edge of accreting torus), r_s is related to thickness $\widehat{\mathbf{h}}_s$ of the accreting matter flow as in Figure (11). r_{mbo} is the marginally bounded orbit. Ω_K^+ has been considered for the counterrotating fluids. The maximum location of inner edge is $r_\times \lessapprox r_{mso}$.

Table 2. Quantities O and $\mathcal{P}$. $\mathcal{L}_\times/\mathcal{L}$ stands for the fraction of energy produced inside the flow and not radiated through the surface but swallowed by central **BH**. Efficiency $\eta \equiv \mathcal{L}/\dot{M}c^2$, $\mathcal{L}$ representing the total luminosity, $\dot{M}$ the total accretion rate where, for a stationary flow, $\dot{M} = \dot{M}_\times$, $W = \ln V_{eff}$ is the potential of Eq. (7), Ω_K is the Keplerian (relativistic) angular frequency, $W_s \geq W_\times$ is the value of the equipotential surface, which is taken with respect to the asymptotic value, $W_\times = \ln K_{\max}$ is the function at the cusp (inner edge of accreting torus), $\mathcal{D}(n,\kappa), C(n,\kappa), \mathcal{A}, \mathcal{B}$ are functions of the polytropic index and the polytropic constant.

Quantities $O(r_\times, r_s, n) \equiv q(n,\kappa)(W_s - W_\times)^{d(n)}$	**Quantities** $\mathcal{P} \equiv \frac{O(r_\times, r_s, n) r_\times}{\Omega_K(r_\times)}$
Enthalpy − flux $= \mathcal{D}(n,\kappa)(W_s - W)^{n+3/2}$,	**torus − accretion − rate** $\dot{m} = \frac{\dot{M}}{\dot{M}_{Edd}}$
Mass − Flux $= C(n,\kappa)(W_s - W)^{n+1/2}$	**Mass-accretion-rates** $\dot{M}_\times = \mathcal{A}(n,\kappa) r_\times \frac{(W_s - W_\times)^{n+1}}{\Omega_K(r_\times)}$
$\frac{\mathcal{L}_\times}{\mathcal{L}} = \frac{\mathcal{B}}{\mathcal{A}} \frac{W_s - W_\times}{\eta c^2}$	**Cusp-luminosity** $\mathcal{L}_\times = \mathcal{B}(n,\kappa) r_\times \frac{(W_s - W_\times)^{n+2}}{\Omega_K(r_\times)}$

bined effect of the increasing **SMBH** spin, and the approaching of $(r_s, r_\times)$ to the central attractor, which means an increase of the dragging effects. Viceversa, in the counterrotating tori, there is $\partial_{a^*}(G^+|_{\bar{\mathbf{p}}_F^{(2)^+}} - G^+|_{\breve{\mathbf{p}}_F^{(2)^+}}) \approx 0$, where $G^+|_{\bar{\mathbf{p}}_F^{(2)^+}} \geq 0\ G^+|_{\breve{\mathbf{p}}_F^{(2)^+}})$, which may be read saying that the O and $\mathcal{P}$ quantities for the counterrotating case are less dependent on the **BH** spin-up process then the corotating ones. Note that in the corotating tor case there is a sharp increase with the **SMBH** spin a/M as $a \gtrsim 0.9M$, and for these value of the spin of the central attractor, some tori can be formed in the ergoregion, or be partially contained in the ergoregion–Sec. (A). Then, as the accretion rate ($\mathcal{P}$-quantity) is larger for corotating then for counterrotating tori (in the adopted parametrization), and increases with the **SMBH** dimensionless spin for corotating fluids, while decreases for counterrotating ones, this implies that the corotating tori may represent very good candidates to explain the **SMBH** mass according to the process considered in[98,99,100,101, 102,103,104], rather then the counterrotating ones[8].

4.4.1 Structure of polytropic tori

In this section we develop some general considerations on the equation of states and the polytropic **RAD** tori, which has been used in Sec. (4.3) for the study of $\mathcal{P}$ and O quantities. Geometrically thick tori consider the hypothesis of a barotropic law $p = p(\varrho)$, this is also used in more general situation where the magnetic field contribution is included in the torus force balance [52,68]. The entropy distribution depends on the initial conditions of the system and on the details of the dissipative processes, and it is constant along the flow. Focusing on polytropic tori regulated by the equation of state: $p = \kappa\varrho^\gamma$, where $\kappa > 0$ is a constant and γ is the polytropic index, in [67] it has been shown that for the Schwarzschild geometry ($a = 0$) there is a specific classification of eligible geometric polytropics and a specific class of polytropics is characterized by a discrete range of values for the index γ–see also [66]. Nevertheless, most of the considerations traced out for the static attractors, $a = 0$, holds also for a more generic effective potential function, in particular for a Kerr **SMBH** where $a \neq 0$– ultimately a similar classification of the polytropics for $a = 0$ was proved to be valid also in the rotating case of the Kerr geometry–[26]. Here we recall some of those considerations in the **RAD** framework, in particular in the case of ℓcounterrotating couples. Using Eq. (7), we can write the density ϱ as function γ. Therefore, we can propose a general classification for the tori $(\mathrm{C}, \mathrm{C}_\times)$, as for proto-jets $\mathrm{O}_\times$, assuming a particular representation of the density function. However, concentrating our attention on the **RAD** components C and $\mathrm{C}_\times$ for which $K < 1$, there is :

$$\varrho_\gamma \equiv \kappa^{1/(\gamma-1)} \bar{\varrho}_\gamma \quad \text{and} \quad \bar{\varrho}_\gamma \equiv \left[\frac{1}{\kappa}\left(V_{eff}^{-\frac{\gamma-1}{\gamma}} - 1\right)\right]^{\frac{1}{(\gamma-1)}} \quad \text{for } \gamma \neq 1$$
$$\text{thus} \quad \varrho_\gamma \equiv \mathbb{C}^{1/(-1+\gamma)}, \quad \mathbb{C} \equiv (V_{eff}^{-2})^{\frac{\gamma-1}{2\gamma}} - 1. \tag{24}$$

Then $\mathbb{C}$ is actually a function of $K \in]K_{\min}, K_{\max}]$, where $K_{\max} < 1$, regulating whether the torus is quiescent or in accretion. Then we concentrate on the case $K < 1$ with the condition $\varrho > 0$; this case is verified, according to Eq. (24), when $\gamma > 1$ [9]see also the ranges[10] in Eq. (12). In the case of very small tori, i.e. with small elongation λ on the equatorial plane, the hydrostatic pressure component is less relevant for the force balance, and the torus approaches the geodesic limit of a one-dimensional (stable) ring of dust (test particle approximation as the pressure forces vanish). On the other hand, keeping the minimal condition $\bar{\varrho}_\gamma > 0$ for the $(\mathrm{C}, \mathrm{C}_\times)$ tori, there is $\partial_k \bar{\varrho}_\gamma < 0$, for any polytropic index. In the limit of large κ, in each point of the torus in equilibrium or in accretion, the pressure and the

[8] However comparing the counterrotating and corotating accretion we need to analyse more carefully the accretion flow. The counterrotating case is in fact a special case of accreting flux where a reversal of flow rotation close to the **BH** (near the ergosurface) is expected. In this sense the spin of a black hole has a special role on the determination of the accretion flow as well as of the accretion rate see [106, 55,107,108,109]. In the evaluation of the quantities in Table (2) we based our analysis on the assessment of the flow thickness which in our model depends on the cusp location, the specific angular momentum and the parameter K, and the quantities $\mathcal{P}$ depend on the fluid relativistic angular frequency at the cusp. We consider accretion flow from the outer counterrotating torus of a $()^- < \mathrm{C}_\times^+$ couple, the counterrotating flow impacts on the inner torus which is generally close to the outer torus cusp (the maximum limiting tori separation is $\bar{\lambda} \approx 8M$ in the geometry of near extreme Kerr **BH** with $a = M$).

[9] The boundary conditions have been fixed so that the tori inner and outer edges are $[r_{in}, , r_{out}] \subset]r_+, \infty]$; this may be read as the extensive range of existence for $V_{eff}(\ell)$. The case $\gamma = 1$ is considered apart where $\varrho_k \equiv V_{eff}^{-(1+k)/k}/(1+k)$ and at the boundaries $\varrho_k^{out} = \varrho_k^{in}\left(V_{eff}^{out}/V_{eff}^{in}\right)^{-(1+k)/k}$,–see the [26].

[10] For any $\kappa > 0$ and $\gamma > 1$, there is the density $\bar{\varrho}_\gamma = 0$ in the limit of large r (i.e. $r \gg r_{cent}$) where $V_{eff} \approx 1$. We should note that equally this is also the case of the boundary configuration for the open $\mathrm{O}_\times$ Boyer surfaces, where the minimum pressure (and density) point is located in $r_\jmath \geq r_{mbo}^{\pm}$ correspondent to $K_\jmath \geq 1$, an overflow of matter in funnels of material occurs [28].

density decrease to zero (with the torus volume). The pressure p, associated to the solution in Eq. (24), depends on $k^{\frac{1}{1-\gamma}}$. It decreases with κ more slowly then ϱ.

We conclude this section with some additional considerations on the role of the density function ϱ_γ and the K-parameter in the **RAD** framework. We consider **RAD** potential $V_{eff}^{\mathbf{C}^2}\Big|_K$ in Eq. (12), for a couple of tori, where, for a fixed distribution of fluid specific angular momentum, $\{\ell_i\}_{i=1}^n$, we can set the fixed parameters (K_i, K_o), defining the boundary conditions in $V_{eff}^{\mathbf{C}^2}\Big|_K$ and used to describe the **RAD** K_ℓ-modes. The function ϱ_γ, for each **RAD** component, is actually function of K. To fix the **RAD**, it is important to consider the ratio K_i/K_o for two adjacent tori–[27, 29]. Using this approach, we finally can obtain a series of constraints related directly to the density functions ϱ_γ, rather then on the K parameters. In fact, as mentioned in Sec. (2), the surfaces of constant density coincide with the constant pressure and potential surfaces. Taking explicitly into consideration Eq. (24), one has for a torus that $K = \left[(\varrho_\gamma)^{\gamma-1} + 1\right]^{\gamma/(1-\gamma)}$.

Then the relation $K_i + \epsilon K_o = \chi$=costant implies for the tori $\mathrm{C}_i < \mathrm{C}_o$, that

$$\varrho_\gamma^i = \left[\left(\chi - \epsilon\left[(\varrho_\gamma^o)^{\gamma-1} + 1\right]^{-\frac{\gamma}{\gamma-1}}\right)^{\frac{1}{\gamma}-1} - 1\right]^{\frac{1}{\gamma-1}}, \qquad (25)$$

with ϵ =constant.

Theory of accreting tori adopted here implies on the other hand that each ϱ_γ^i and ϱ_γ^o are constant. Finally, to simplify our arguments, we have assumed that the polytropic indices (but not necessarily the polytropic constant κ) are equal for each torus. This hypothesis may be especially relevant for the ℓcorotating couple. Note that we can then directly impose several constraints for the density function. Some simple examples, including special (composite) density profiles are, for example, the case $\varrho_{[+]}^- = \varrho_\gamma^i - \varrho_\gamma^o = \varrho_\Phi$ =constant, where

$$K_i = \left(\left[\varrho_\Phi - \epsilon\left(K_o{}^{-\frac{\gamma-1}{\gamma}} - 1\right)^{\frac{1}{\gamma-1}}\right]^{\gamma-1} + 1\right)^{-\frac{\gamma}{\gamma-1}}.$$

These solutions create special tori surfaces from the condition on the constant pressure. Moreover, within the limits considered before, these constraints can found application also in the collision analysis, to infer the final states (es. final merger tori) from these constraints[11].

5 General discussion on interacting tori and energetic of associated processes

This first evaluation of the energetic related to the tori collision processes, performed by considering colliding particles associated with the **RAD** tori, certainly suggests a promising and interesting aspect of the agglomerate energetics. Here we add some clarifications about these processes more specific in the **RAD** framework collision they are associated to. Situations showed in Fig. (14) deal basically with two very distinct phenomena depicting the tori collisions, the first **−j−** concerns the only couples $\mathrm{C}_\times^- < \mathrm{C}_\times^+$ or $\mathrm{C}^- < \mathrm{C}_\times^+$ (as there must be an inner torus screening between the central **BH** and the accreting outer torus), and arises due to the matter overflow from the cusp of the outer accreting torus, which impacted onto the inner corotating torus. The second process **−jj−** instead does not necessary involve accretion from the outer torus, and the main process features an impact from the quiescent or accreting outer torus on the inner one or, more precisely, a contact between two adjacent tori of the couple, as such they may involve ℓcorotating or ℓcounterrotating tori, thought the conditions for such collisions to occur turn to be constrained especially by the **BHs** dimensionless spin defining some special **BHs** classes. We will add some further comments on this collision mechanics below.

Focusing on the **−j−** case, the initial state of the inner torus is in fact not relevant for analysis of this very initial phase of collision and the assessment of the conditions for a collision after accretion from the outer torus. In the case where the outer torus is in accretion, collision is driven by the dynamics of the external torus, the inner torus acts as a screening mass between the accreting torus and the central black hole, similar situations are for example considered in [12, 13, 14, 15, 17]. Clearly the initial state of the inner torus is relevant in the second phase of the collision mechanisms, when we are forced to explore the situation under a wider perspective to consider the final state of the **RAD**. In the **−j−** mechanism, the spacing region $\bar{\lambda}_{i,o}$, defined as in Fig. (7), plays an essential role together with the initial constrains on the outer torus. Both aspects are thoroughly discussed in Sec. (3).

Nevertheless, the evaluation of the energetics of collision processes in the **RAD**, either for **−j−** or **−jj−** mechanism, cannot avoid a more general, global approach, by considering collision as a "global" phenomenon involving matter flow from the outer torus and a large part of the inner torus, rather then focusing on each particle of the flow. On the other hand, the amount of matter overflow from each accreting torus, may also be affected by the accreting torus (global) oscillations; we do not consider here this aspect, but we refer for example to –[52].

We now concentrate on the **−j−** case, particularly on the ℓcounterrotating $\mathrm{C}_\times^- < \mathrm{C}_\times^+$ as seen in Fig. (14), which pictures the outer torus as source of accreting matter falling onto the inner one. More specifically, regarding the (**−j−**) mechanism, we should consider the outer torus mass accretion rate $\dot{M}$ and matter flux, as well as the flow thickness, defined in Table (2) and carefully studied in Sec. (4.3). These quantities are functions of the **BHs** spin and range of variation of the the fluid specific angular momentum. Therefore, in this investigation we find the maximum and minimum values of these quantities, for given initial conditions on the outer (counterrotating) torus. These aspects are all considered in Sec. (4.3), where we also refer to a direct and explicit comparison between the corotating and counterrotating tori. Some additional notes about the free-particle assumption for matter leaving the cusp are also included, this hypothesis is translated into the use of Keple-

[11] Other notable cases might be founded by the constraints $\varrho_{[\times]} = \varrho_\gamma^i \varrho_\gamma^o$ =constant, $\varrho_{\{\times\}} = \varrho_\gamma(K^i K^o)$ =constant or $\varrho_{\{+\}}^\pm = \varrho_\gamma(K^i \pm K^o)$ =constant. It is possible to show that not all these profiles are related to quiescent of accreting toroids.

rian velocity for the particle. We are not concerned here with the conditions, or the **RAD** evolutive path, leading to a possible couple $C^-_\times < C^+_\times$ which are investigated in [29] and considered also in Sec. (2), nevertheless the initial conditions on the density mass and angular momentum are necessary for the evaluations of all the quantities of Table (2). For the evaluation of the mass accretion rate, cusp luminosity and other relevant quantities of accretion tori, we assumed also the inner and outer tori are filled with polytropic fluids, and in Sec. (4.4.1) we revisit this hypothesis, the polytropic equation of state allowing to rewrite in an explicit way the density ρ in terms of the K-parameter. The tori morphology, the thickness and elongations of each component of the couple is constrained in Sec. (3), the morphology of the aggregate components are important to asses the possibility of tori collision, the state of tori (if quiescent or in accretion) and in general the **RAD** instability. This information provides also some hints on the density of the fluid, as the K parameter is directly linked to the torus density. We shall see that some rather small tori may be described as well by the model adopted in the investigation for each **RAD** component, especially for the ℓcounterrotating couples $C^-_\times < C^+_\times$, according to specific classes of **BHs** attractors –Sec. (4.3). Actually small **RAD** tori of this kind of couple are expected to be especially characteristic of slow rotating and low mass attractor. Construction of accretion models have narrowed many of the relevant features of geometrically thick disks and particularly of the so called Polish doughnuts which are very close to the models adopted for the **RAD** components. There is a certain variability in featuring such tori, depending essentially on the central attractors (as it is the case also for the **RAD** model), and on the force balance condition regulating the **RAD** dynamics. Generally, these tori are opaque, having extreme optical depths. Expected to be cold, such tori have temperature less or much less than the virial temperature. They are radiation pressure supported and cooled by advection with low viscosity. Very importantly for the **RAD** energetic is that geometrically thick tori are characterized by high accretion rates, with super-Eddington or highly super-Eddington luminosity (with very small accretion efficiency). We refer to Sec. (4.3) for evaluation of related quantities in dependence of the parameters (ℓ, K) and the **BH** dimensionless spin. We know the entropy is constant along the flow, the enthalpy flux has been investigated in Sec. (4.3). We remind nevertheless that super-Eddington accretion, thought often associated to strong matter outflows, does not *necessarily* imply this, and this fact turns to be very significant in the modeling the processes of the **BHs** seeds growing towards the **SMBH** sizes to justify the masses of these extreme compact objects at high redshifts. A further explanation on the other hand involves different accretions stages of the **SMBHs** accretion tori life, and this particular mechanism is in fact seen here as one of most promising situations in which **RAD** structure can be directly involved through several accretion stages induced by **RAD** instability. Given the importance of this aspect for the energetic of the **RAD** processes, and for the mechanisms of accretion of medium-small masses **BHs** towards **SMBH** at high redshift, we have dedicated Section (4.3) to the study of these quantities, focusing nevertheless on stressing the distinction between corotating and counterrotating tori. The initial conditions, prior to the collision, i.e., the range of values for the specific angular momentum ℓ of the two tori and the parameter K, have been dealt with in dedicated works. The assessment of the initial (i) parameters $(\ell_i(i), \ell_o(i))$ are then important for the evaluation of the energetic of the process and the range of density values for the fluid and the tori elongation on the equatorial plane. While not specificized otherwise, we shall indicate (i) for initial and (f) for a final state of a process. The ℓcounterrotating couples can have different evolutive paths according to initial data con angular momentum, with respect to the **BH** spin, and to the fact that the angular momentum may change magnitude, remaining in **L1**, or it can possibly increase up to values in **L2** or **L3**. Nevertheless, these possibilities turned to be significantly constrained by the **SMBH** dimensionless spin[12] [29].

If the outer torus is counterrotating, we may assume the falling material delivers negative angular momentum, increasing the mass of the inner accreting torus (possibly affecting K_i parameter) and, simultaneously, lowering its angular momentum; this is based on the simplest assumption that $\delta\ell_i \equiv \ell_i(f) - \ell_i(i) \leq 0$, where in the final (f) state, $\ell_i(f)$ is taken almost constant. The lowering of the angular momentum magnitude of the inner torus in principle would imply a increase of the cusp location (and of $K_{\max}$) and a decrease of the torus center as well, i.e., $r^-_\times(f) > r^-_\times(i)$ and $r^-_{cent}(f) < r^-_{cent}(i)$–see Figs (13). But this aspect comes into competition, as we will discuss below, with the simultaneous mass increase, which may correspond to a change in K (this is actually a function of matter density, but also of the torus specific angular momentum). Moreover, under suitable conditions it could also turn to block the accretion of the inner torus. If the cusp moves inwards, the increase of the torus mass m^-, due to the new injection of matter from the outer torus occurs, and the simultaneous decrease of specific angular

[12] A state of a **RAD** component is fixed when the parameters (K, ℓ) and the tori morphology are established. The possibility that a **RAD** couple may also return to a previous state of the evolution path was named *state loop* in the couple evolutionary graph in [29]. Considering the results traced in [29], we briefly summarize the general constraints on the fluid specific angular momentum and the **BH** dimensionless spin for any state of the couple $()^- < ()^+$, made by an inner corotating torus and outer counterrotating torus. These constraints were then discussed together with the constraints on the K-parameters–see also [27]. First, let us introduce the **BHs** spins $a_t = 0.3137M$ and $a_0 = 0.3726M$, the last spin has also been introduced in Sec. (4.2) see also Fig. (14). These spins, rather close in values, refer to slowly spinning **SMBHs** with respect to the limiting spins considered in Eq. (11). In [29], we introduced the concept of correlation which here is intended for occurrence of the possibility of tori interaction, or a tori collision. The situation is as follows: Couple $C^- < C^+_\times$ is clearly in correlation while for the situation of $C^-_\times < C^+$, with an inner torus in accretion and an outer quiescent torus, only sufficiently slow **BHs**, $a < a_0$, can be characterized by the couple correlation. If the inner torus is in a proto-jet unstable phase, collision never occurs, unless the outer torus is not in accretion, or a proto-jet for attractors with $a < a_t$. On the other hand, the situation when an outer torus is a proto-jet with an inner (corotating) torus in accretion be only be observed in the spacetimes with $a > a_0$, and there is no tori collision. In the state with both proto-jets, collision is possible only for $a < a_t$; if the outer configuration is a proto-jet and the inner torus is in equilibrium, then there is a collision. Viceversa, if the outer torus is in equilibrium, and the inner structure is a proto-jet no correlation occurs.

momentum may also lead to an decrease of the accretion rate. However, Sec. (4.3), and especially the analysis in Figs (15), presents particularly the behavior of accretion rate with respect to the cusp location and the specific angular momentum.

This dynamics on the other hand concerns also the second tori collision process, $-\mathbf{jj}-$, occurring when $\bar{\lambda}_{i,o} = 0$, and the collision is due to two possible evolutive paths of the colliding couple or a combination of the two: in the first, $-\mathbf{jj_o}-$, collision is caused by the outer torus which, in accretion or quiescence, stretches onto the equatorial plane, $r^o_{in}(f) < r^o_{in}(i)$; this change can happen for a change in the angular momentum magnitude (thus $r^o_{cent}(f) < r^o_{cent}(i)$), or a net increase of the K-parameter at ℓ approximative constant (thus $r^o_{cent}(f) \approx r^o_{cent}(i)$ and $r^o_{in}(f) < r^o_{in}(i)$, while $r^o_{out}(f) > r^o_{out}(i)$ and the torus elongation $\lambda^o(f) > \lambda^o(i)$) or a combination of the two–[29]. The second $-\mathbf{jj_i}-$ is due to the inner torus which is growing $\ell^-(f) \approx \ell^-(i)$ or stretching towards the accretion at approximative constant K_i, or viceversa an increases of $K^i \approx K^i_{\max}$ at ℓ^i almost constant (with also $r^i_{out}(f) > r^i_{in}(i)$) implying arising of an accretion phase for the inner torus. Processes $-\mathbf{jj_i}-$ and $-\mathbf{jj_o}-$ may be therefore described also in the framework of ℓ-modes or K_ℓ-modes respectively. They result in an ultimate stretching in the equatorial plane where r^i_{out} moves outwards, thought not necessarily r^i_{cent} grows, or viceversa, with an increases of ℓ^i, and a shift outward of r^i_{cent}, leading to $\bar{\lambda}_{i,o} = 0$. A general discussion of the evolutive processes of the couple can be found in [29] while we shall draw here some qualitative considerations, more specifically on the conditions *after* collision. Thought we do not approach directly the modeling of the collision phenomena between the fluid of the two tori requiring a different approach being a task far from the one considered here, we note that, for this purpose, it is in fact essential to fix the initial conditions on the colliding couples, as we have done in the evaluation of the test particle collision. A colliding couple $\mathrm{C}^-_\times < \mathrm{C}^+_\times$ can lead to a state after the collision made by one torus or two final tori i.e. **-I-** a **RAD** made up by one torus, $()^\pm$, with final state described by parameters $(\ell(f), K(f))$ or $-\mathbf{II}-$ a couple $()^- < ()^+$. Note that the tori state in **-I-** and **-II-** has not been specified as it could be in accretion or quiescent. However, assuming the background spacetime remains unaltered during the process, i.e, the accretion matter does not change the spin or mass of the central attractor neither the torus self-gravity leads to a feedback reaction these situations are in reality very much constrained by ℓ and a further analysis bounds the relative values of (K^i, K^o) in the final states. Then, as considered in [29] the second evolutionary path, $-\mathbf{II}-$, could be also a transient stage leading finally to one torus, $-\mathbf{I}-$, or generally being part of a series of further evolutionary phases, where the couple is subject to different state transitions. In the case $-\mathbf{I}-$, a one torus solution can be found when, either because of in accretion (decreasing its angular momentum magnitude at almost constant K), or for growing gaining a greater value of K, the outer torus may eventually merge with the inner resulting in a single torus, destroying the **RAD** and carrying the system to the commonly considered accretion environment when a central **SMBH** is surrounded by one orbiting accretion torus. It is clear that these considerations enter also in the discussion of the processes of the **BHs** accretion tori formation.

$-\mathbf{II}-$ In the case where the final state is made by a couple of tori, we concentrate on the situation for the inner torus with parameters $(\ell(f), K(f))$, discussing briefly the situation for the outer torus also. Two main processes are in competition :**(a)** on one hand there, is an increase of matter provided by the outer torus such that $K(f)$ is the new parameter value for the inner torus and $m(f)(K(f)) > m(i)(K(i))$ where m is the torus total mass. One evolutive path can feature an outer torus which is losing mass and momentum approaching the accretion (the torus being smaller), while matter impacting on the inner torus may be not sufficient for accretion to occur, i.e., to lead to a situation were $K_i(f) < K^{max}_i(\ell_i(f))$. This inequality has to be evaluated together with $\ell(f)$ and $\ell(i)$. However, it should be also considered that this situation does not necessary occur, because in fact in the evaluation of the role of the $K(f)$ parameter actually what is most relevant is the value of $K(f)$ related to the limits $[K_{mso}, K_{\sup}[$ (or more precisely $[K_{\min}, K_{\sup}[$), where $K_{\sup} = K_{\sup}(\ell)$ is a function of the specific angular momentum at fixed **BH** spin. Therefore the problem of change in the inner torus rotation law has to be addressed prior the evaluation of mass increase. Nevertheless, the initial and final state of each torus can be studied in fact as an ℓcorotating couple (the states of the single torus before and after the collision do not change the direction of rotation with respect to the black hole, changing only in magnitude of the specific angular momentum). An increased $K(f) > K(i)$ for $\ell(f) > \ell(i)$ does not lead necessarily to an increase of the torus elongation and the establishing of the accretion (precise limits and methods are in [27]), while there is $r_{center}(f) > r_{center}(i)$ for the tori centers and $r_\times(f) < r_\times(i)$ for the tori accreting points, thus, if the inner torus acquires enough mass from the outer torus such that $K(i)(\ell(i)) + \Delta_K = K(f)(\ell(f))(r_{\max})$ and $\ell(f) \in \mathbf{L1}$, then there is $\lambda(f) > \lambda(i)$ and the accretion of the final state of the inner torus can lead to collision with the outer torus. This holds also if the outer torus loses its angular momentum, $|\ell^+|$, entering a phase where $\lambda(f) < \lambda(i)$ and there is $r_{cent}(f) < r_{cent}(i)$ for the tori centers. However, in this dynamical process constrains on K will remains decisive. It is clear that the specific angular momentum after collision is the first significant parameter to fix the state, as K depends on the limits on ℓ and $K(f)$, and on the difference $\Delta K(f) \equiv K_{\sup}(f) - K(f) = \Delta K = K_{\sup}(i) - K(i)$. Accreting matter brings also specific angular momentum, then assuming that the outer torus is small, we may assume $\ell(i) \approx \ell(f)$ while $K(f) \leq K(i) + \Delta K_{i,f}(r^o_s, r^o_\times)$ where $\Delta K_{i,f}(r^o_s, r^o_\times)$ is a function of the quantity of matter accreting from the outer torus on the inner. Actually, the relation between the specific angular momentum (ℓ^+_o, ℓ^-_i) is properly fixed, the maximum elongation of the outer and inner tori, their thickness, their spacing, and ranges of specific angular momentum, are constrained by the central attractor dimensionless spin. Quantity $\Delta K_{i,f}(r^o_s, r^o_\times)$ is dependent also on the cusp location (which may vary), and location of r_s; this radius enters through the quantity $W(r_s)$: $W(r_\times) < W(r_s) < 1$, and it is related to the thickness $\overleftarrow{\mathbf{h}}_s$ of the accreting flow, analyzed in Sec. (4.3), see also Fig. (11). Therefore, all these quantities will depend on the difference $\Delta W = W(r_s) - W(r_\times)$. Note that generally the outer torus may be far more larger then the inner one as the **BH** spin increases.

Since these processes can involve a substantial part of the inner torus, it is necessary to discuss the situation for the inner

torus of the couple to trace some conclusions on the **RAD** final state after collision. On the other hand, in the **RAD** framework, tori dynamics cannot generally be effectively considered for tori being disentangled. It is possible to consider the evolution of each torus disentangled from the others only in some periods of the **RADs** evolution. The possibility that tori of the aggregate do not collide, evolving independently from each other is expected to the especially relevant for super-massive Kerr **BHs** and Kerr **SMBHs** with near extreme dimensionless spin.

In this regard, we conclude this section by discussing a further relevant aspect to be consider in the energetic involving a **SMBH** interacting with orbiting tori. These objects can be subjected to the runaway instability, a phenomenon, here directly affecting only the **RAD** inner accreting torus, but indirectly the entire couple. Therefore, the couples where runaway instability may arise are $\mathrm{C}^{-}_{\times} < ()$, or $\mathrm{C}^{+}_{\times} < \mathrm{C}^{\pm}$, as these may involve either corotating or counterrotating torus. The runaway instability is due to the interaction of the **BH** with the accreting torus via accretion of matter flowing into the **BHs**. The basic mechanism features an interactive dynamical model involving both the attractor and the accreting torus: basically because of the change in the mass **BH** parameter, the accreting torus cusp can move deeply towards the torus, i.e. the tori accreting points are related by $r_{\times}(f) > r_{\times}(i)$ where i and f are for initial state prior accretion and f is for the torus state when runaway occurs. Note that we do not explicit the role of the torus center (implying explicitly a torus angular momentum change). These effects can be specially relevant in the **SMBH** accretion processes. Increasing the mass lost rate $\dot{M}$ due to the cusp will bend inside the torus. The black hole parameters and specifically **BH** mass increase, depending on the mass accretion rate and the matter impacting on the **BH** event horizon. Consequently, the spacetime structure is modified, and this also implies decreasing the spin-to-mass ratio. In terms of **RAD** dynamics, there can be a shift from an attractor class to another [30,29]. Consequently the accretion tori and then the **RAD** never reaches a steady state. Actually, a similar mechanisms of **BH**-accreting torus interaction can arise also after a spin-shift, and more generally, this feedback process from the **BH** should be seen together with any other phenomena involving any change of the **BH** parameters, spin and mass (and eventually even symmetries). Nevertheless, from the point of **RAD** morphology structure, the cusp may also move inwardly towards the black hole, decreasing the mass transfer, and therefore stabilizing the entire process (see for the dependence of the accretion rate on the cusp location and other parameters the analysis of Sec. (4.3)). Viceversa, there is the occurrence of the runaway instability when the cusp moves outwards, penetrating the torus, resulting finally in an increases of mass transfer rate. Note that the accreting torus could even be completely destroyed by such instability. From methodological point of view, the study of this situation can be carried out by considering stationary models [110]. This can be interesting for the applications of this approach to **RAD** environments and this method in fact is also applied in the analysis of the **RAD** possible evolutive paths discussed here: in our language the inner torus $\mathrm{C}^{i}_{\times}$ releases a part of its mass, with a total loss of $\mathfrak{F}_K K(i)$, and angular momentum $\mp\mathfrak{F}_\ell \ell^{\pm}$ (where $\mathfrak{F}_K \ll 1$ and $\mathfrak{F}_\ell \ll 1$) to the central attractor which swallows it, the final stage of this first part of the process is then concluded and a new calculation can consider further state with a new background, which is changed after change of the **BHs**, the new position of the cusp is then evaluated. Generally, the study of this phenomenon can be performed in a non-dynamical framework. The evolution of the central black hole is read as a sequence of exact black holes solution, each picture of the sequence being labeled with a different mass, whose increase is function of the mass accretion rate. Consequently, following the dependence of the mass accretion rate (see Sec. (4.3)), the runaway instability is regulated by several parameters, from the **BHs** dimensionless spin, to the cusp location, the flow thickness and ultimately by the structure of the innermost part of the torus. Pictures of the systems during stages of its dynamics was studied, this method was carefully analyzed and discussed for geometrically thick torus around Kerr **BHs** in [26]. Here we apply this approach to the characterization of the **RAD** dynamics. The relevance of the runaway instability for the **RAD** dynamics should also consider the process time-scales (which in general is considered to be short, depending also on different parameters and especially the attractor) compared with the time-scale of the dynamical processes of the accreting torus model, and in the **RAD** framework, of the **RAD** dynamics. In a system made by a **RAD** couple and its **BH** attractor as in Fig. (14), while the accretion from the inner corotating torus may establish the runaway instability, this can be accompanied by a further process of torus-torus interaction, which would bring, according to the mechanisms considered above, also a change in the cusps, and if a runaway of the inner torus is established, then also the outer torus is affected. Similarities between **BH**-inner torus runaway process, and the mechanism of torus-torus interaction appear. The consequences of tori collision may analogously lead the evolution of both the elements of the mechanism, going through a positive or negative feedback reaction. One of these stabilizes the torus and the couple process, the other turning in a more complex situation where evolutive loops may also occur, giving rise also to more accretion cycles–a mechanism supposed for example in [29]. This is particularly interesting in the case of double accretion, or accretion from outer counterrotating torus, where the presence of an screening quiescent inner corotating torus blocks the runaway from the outer torus accretion. In this respects we could talk about torus-torus and torus-**BH** runaway instability. A torus-torus runaway may be seen as analogue problem with respect to the **BH** runaway instability, not concerning, however, the background spacetime. The runaway instability has also been considered playing a part in the **GRB** production, and more generally in the energy extraction from the central **BH** engine, released by the accretion mechanism itself together with the extraction of the rotational energy of the rotating black hole via the Blandford-Znajek mechanism. All these aspects could be combined in the **RAD** scenario with the dynamics of the interacting tori.

6 Conclusion and future perspectives

The physics of accretion around super-massive black holes has been extensively studied, both on a theoretical ground and by means of numerical simulations bringing knowledge of both the accretion disk dynamics, inherently disk formation and disk

instabilities. These studies have often dealt with issues which are partially still unresolved, as a full description of the accretion mechanism or even jet launching. A complete physical picture of all these phenomena around strong attractors remains to be framed in a unique setting, since there are strong signals that there should be some unique interpretive framework to deal with the pieces of the accretion puzzle. Here we concentrated our attention on the possibility that more than one accretion configuration, a couple of tori, may be formed around a central super-massive Kerr **BH**. Similar structures are considered as screening bubbles of dust or other materials in studies of X-ray **BH** emission. Analogue effects produced by generic cloud might arise from configurations considered here, taking care to consider axial symmetries and coincidence of the orbital plane with the equatorial plane (the specific toroidal model considered here as **RAD** component is also optically thick). Up to now some ad hoc mass distribution additional to the main accretion disks was considered, avoiding a discussion of structure, morphology and more general constraints–see [111, 112, 113, 116] where titled and strongly misaligned disks are considered. In a broader perspective of analysis one might think that some aspects on the **AGN** activities, connected to the formation of such materials (and especially optically thick material), may fit to an adaptation to the **RAD** context. Cloud accretion has been also claimed as a mechanism, together with star tidal disruption, to enhance the **SMBH** accretion rate–see for example [114]. The other possible case, represented by a series of small and random accretions, overlaps with the predicted **RAD** evolution phases due to its inner ringed structure. Screening effects of X–ray emission have been instead studied for example in [11, 12, 13, 14, 15, 16, 17]. Such investigation also suggests that optical and X-ray emission profile obscuration may arise from different phenomena caused by several materials including dust surrounding the inner part of the galactic nuclei, randomly distributed around the central **BH**. Depending on the gas density, the light emitted could be absorbed in the optic and in the X-ray electromagnetic band, distinguishing **AGN** as obscured, not obscured, or much obscured (or *Compton thick*)-see also recent analysis [115]. Assuming a **RAD** scenario one could analyse this obscuration. The observed tori are constrained as the inner torus of the **RAD**, or the inter–torus (quiescent and corotating), located between two tori where the outer (counterrotating) one is accreting towards the central attractor. Although certainly more detailed studies focused on this aspect are necessary, a screening torus proposed here could not be excluded in our opinion as a concurrent cause of the obscuration effects.

This work bridges this gap with the aim to provide a reliable general set of constraints on the ringed disks and emerging instability. This analysis led also to three sideline results: ***1.*** a very first evaluation of the energy release after tori collision from two colliding tori of the same **RAD**, according to two different collision mechanisms discussed in Sec. (4.2), proving that energy release in such phenomena may be really huge depending on the attractor rotation. ***2.*** Second, the results trace a link between the attractor characteristics and the orbiting tori helping, on one side, to determine the model to be adopted and to distinguish the central **BH** with its associated **RAD**–Sec. (2). ***3.*** Third, we provided an extensive comparative study of properties of the counterrotating accretion tori orbiting around a Kerr **SMBH** with respect to the corotating tori. A substantial part of development and especially of analysis of the phenomenology associated with **RAD** features the presence of ℓcounterrotatin couple. Although the hypothesis of having counterrotating tori has been considered in the literature, most studies are predominantly oriented towards the analysis of the corotating accreting tori interacting with their central spinning attractor. On the other hand, the **RAD** investigation made it necessary to explicitly address the possibility of the formation of counterrotating extended toroidal matter configurations especially around **SMBHs**. We set constraints on the formation and accretion of such tori, This analysis has also led to a careful assessment of the accretion rate, cusp luminosity and accretion efficiency in dependence of the **BH** spin and the cusp locations for the two classes of orbiting fluids. To our knowledge, this systematic study has been for the first time directly addressed in literature.

In this analysis we have considered every central Kerr black hole attractor: from very slow, up to the Schwarzschild limit, to the limit of extreme Kerr **BH**. We realized a systematic investigation of the parameter space for the tori, with particular attention to the case of tori in accretion and tori collision, providing a classification of couples according to the dimensionless spin of the central Kerr **BH**. We demonstrate that only specific couples of accretion tori can orbit around a central Kerr **BH**–Sec. (4.1). The dimensionless spin of the Kerr black hole strongly constrains the possible couple of orbiting tori in number, location and relative range of variation for specific fluid angular momentum and density parameter. There are strong indications that (see [27, 29, 28]) **RADs** are capable to feature a "co-evolution" of **BH** system and galactic life of the **BHs**, implementing a **BH-RADs** correlation paradigma, relating specially featured **RADs** evolutions to one special class of Kerr **BHs**, according to their dimensionless spin–[30].

The systems investigated here offer several methodological and observational challenges. Describing a set of virtually separated tori orbiting one attractor as an entire configuration, requires a certain number of assumptions. A first aim of this paper was to establish the conditions for the existence and instability of the couple of tori, considering also the possibility of tori collision at a certain stage of the couple evolution. To do this, we adopted both an analytical and numerical approach, considering an effective potential function for the tori couples and by considering a direct integration for certain particular representative cases, guided in the parameter choice by the analysis of geometric properties of the Kerr spacetime. The general relativistic hydrodynamic equations we solved are coupled with proper boundary conditions, enabling to take account of the presence of two tori and eventually emergence of their collision regime. This onset was modified in a simple way in order to preserve the general relativistic hydrodynamic approach for each individual torus which is commonly rendered through an effective potential function. We casted therefore in Sec. (2) the set of the Euler equations using a composite effective potential for the couple.

We believe our study show there is a strong motivation to discuss the results of this approach in comparison with more complex scenarios where the contribution of the radiation, viscous and magnetic factors having a predominant role at least in

some phases of the evolution of the formed structures. For each torus, this implies also the need to define the specific nature and *history* of the **BH** attractor and of each **RAD** component.

The theory of the perfect fluid relativistic torus orbiting a Kerr **BH** has been developed since the first fundamental works in many different applications. For the first time to our knowledge, it is however applied here and in [27,28] to the description of a couple of tori. The results reported in this work are certainly a first step towards the understanding of the dynamics of a tori couple and therefore we expect several different extensions of the model and its improvements. Particularly, we plan to extend the investigation to the scenarios where different rotational laws are considering for the accretion tori. In addition, it would be interesting to investigate, using more elaborated approaches, further situations where, for example, a change of the **BH** parameters is expected due to accretion, or where the tori self-gravity is considered. A possible mechanism expected to be relevant in the case of a thick torus is for example the runaway instability [117], raised eventually from accretion of the inner **RAD** torus (in the ℓcorotating or ℓcounterrotating tori of the kind $C^+_\times < C^-$ or $C^-_\times < C^+_\times$.) As consequence of the mass loss through the cusp of the inner tori, the **BH** parameters would be affected by the accreting material, therefore the spacetime geometry modified and so the instability of the accreting tori occurs, changing its cusp $r_\times$ location. It is worth pointing out that in our model prescription of such runaway mechanism may eventually trigger a drying-feeding process in which the inner torus would be characterized by several stages of instabilities. We should note that each torus in this special **RAD** has high or very high accretion rates; we expect in processes analogue to feeding-drying, this can be give rise to a sort of "clumpy" episodic accretion process. As mentioned above, a further challenge acknowledges the existence of very different **RADs** tori histories which may be distinguished in three periods of **BH**-ringed accretion disk life: the first (**I**) featuring tori formations, the second (**II**) facing the accretion of one or two tori onto the central **BH** and the third (**III**) the eventually emerging of tori due to collisions. Picturing these situations is clearly a complex task. Each of these periods obviously counts on different contributions to the balance of forces for the torus, hence the need to deal with the problem with different tools. We were motivated to provide general applicable results with the least number of assumptions that would make this a very specific model restricted to a particular attractor and particular torus. We substantially reduced the parameter space of our model, providing ranges of variation of the variables and parameters which may fit also to some extent for other models, providing also attractor classes on the bases of the tori features indicating the attractor which we should chase to find evidences for. Dynamics and tori instability are generally determined by the balance of gravitational, magnetic, centrifugal and hydrostatic pressure, together with dissipative effects, as viscosity and resistivity, eventually torus self gravity and radiation pressure. Each of these ingredients is relevant in one of the disk period and mainly determine the disk model to be adopted. On the other hand, the disk model is tightly bounded to the attractor, thus the choice of a geometrically thick accretion torus around a **SMBH** where the curvature contribution to the force balance is predominant, is usually well founded. Setting our analysis in this model, we are able to provide general and strict limits especially on periods **II** and **III**–(a more careful analysis of the evolution of these systems is discussed in [28,29]). By neglecting here the period of formation of the single tori that can be attributed to the influence or combination of different phenomena, we concentrate on the second period and the emergence of the collision. A second aim of this paper, addressed in Sec. (4) was in fact to investigate the emerging of tori collision and the related mechanisms. In all of these catastrophic events, collision energy is expected to be released. An evaluation of CM-energy in the test particles approximation is provided. Although it suffers of various issues (e.g. fine-tuning problems [118]), this approach is effectively widely used as a useful first approximation. In the future investigations, the role of other factors as radiation, magnetic fields, and temperature could be included. As shown in Fig. (14), collisional efficiency of interacting matter of ℓcounterrotating tori increases with increasing **BH** spin being very high for near-extreme **BHs**. Results on collision thus suggest that collisional double tori effects may represent a new and unexpected sources of radiation that might be observed through the phenomenology associated with both the stable and unstable configurations, giving clear indications that considering only part of the expected contribution a large release energy is expected from the collision. The phenomenology associated with these toroidal complex structures may be indeed very wide. This new complex scenario in facts lead to reinterpret the phenomena analyzed so far in the single-torus framework. The radially oscillating tori of the couple could be related to the high-frequency quasi periodic oscillations (**QPOs**) observed in non-thermal X-ray emission from compact objects, keeping fingerprint of the discrete radial profile of the couple structure. More generally instability of such configurations, we expect, may reveal crucial significance for the high energy astrophysics related especially to accretion onto supermassive **BHs**, and the extremely energetic phenomena occurring in quasars and **AGNs** that could be observable by the planned X-ray observatory `ATHENA`[13].

Further important aspect, investing the methodological point of view, concerns the applicability in different contexts from the stationary hydrodynamic model set-up adopted here for the single torus. If this first investigation on tori collisions is to be understood as a proposal where introduction of additional ingredients should be taken into account by specific models for the single torus, we expect that in the balance of different contributions, the presence of other magnetic or viscosity effects cannot qualitatively change the constraints enlightened here. To be certain of adaptability and applicability of the results plotted here, we need to consider first the adaptability to other models of the results concerning the limit of one-torus model. The hydrodynamical model considered here is widely applied in many contexts and surely showing a remarkably good fitting on the more complex models as well discussed for example in [64] when it comes to the analysis of morphology presented here. These results can then be used as initial data and comparative model in any numerical analysis of more complex situations, sharing the same symmetries, as it is generally adopted in many general relativistic hydrodynamic (GRHD) or and general rel-

[13] `http://the-athena-x-ray-observatory.eu/`

ativistic magnetohydrodynamic (GRMHD) approaches for the single accretion disk case. In the current analysis of dynamical one-torus system of both GRHD and GRMHD set-up, the geometrically thick tori considered in this work for each **RAD** component, are commonly adopted as initial configurations for the numerical analysis–[54,55,57]. This is a good hint of the reliability in wider contexts represented by different accretion disks supported by more complex accretion. There is no expectation that there would be a qualitative overcome of constraints provided here, especially for period **II** which are reasonably not *qualitatively* affected by other contributions. The *morphological* features of the equilibrium and locations are certainly predominantly determined in these studies by the centrifugal and gravitational components (see for example the very much debated definition of inner edges of accreting disks, which is commonly accepted running in the range $]r_{mbo}, r_{mso}]$ according to the specific tori model). Thus, this work is also intended to be a guideline for constraints on numerical dynamical analysis.

A further aspect influencing the model development is the **RAD** formation. These coupled tori are expected to form as a result of the interaction of the central attractor with the environment in **AGNs**, where corotating and counterrotating accretion stages are mixed. A major, suggestive possible host-environment for **BH-RADs** are **AGNs SMBHs**. There are evidences suggesting what these **RADs** structures may play a major role in Galaxy dynamics and particularly in **AGNs**. Several studies are in support of the existence of **SMBHs** characterized by multi-accretion episodes during their life-time in Galaxy cores. Consequently **SMBHs** life may report traces of its host Galaxy dynamics as a diversified feeding of a **SMBH**. These processes may involve repeated galaxy mergers or also interacting binary **BH**, X-ray binaries or **SMBHs** binary systems. As a consequence of these activities, matter around attractor could give an equilibrium configuration as counterrotating and misaligned tori [116,112]. Sequences of orbiting toroidal structures with strongly different features as, for example, different rotation orientations with respect to the central Kerr **BH** are argued to be produced from chaotical, discontinuous accretion episodes where corotating and counterrotating accretion stages are likely to be mixed [46,40,45,41,42]. In this environment where also the galactic magnetic field can eventually play an important role in the formation and rotation orientation of each tori, strongly misaligned tori with respect to the central **SMBH** spin may appear [111,112,113,116]. Further phenomena seen as possible candidate for **RADs** formations may be **BHs** kick-out in **BH**-populated Galaxy core–see for example [119]. The turbulent attractor life would be source for very different accreting matter in some kinds of binary systems, or may involve the self gravity of a unique original accreting disk which finally splits into several rings.

From observational view point, we believe our results may be of significance for the high energy astrophysics. In fact the presence of such structures is capable to substantially modify the single disk scenario, which has been effectively taken so far as the interpretative common ground. Explanation of some of most intriguing and unveiled issues of **BHs** physics interacting with matter may be reset in this new framework where single tori paradigma would be then just seen as a limit or special case related to an evolutive phase of non isolated **BHs** life. The presence of inner tori may also enter as a new unexpected ingredient in the accretion-jet puzzle, as proposed also in [34, 35,36] and [28]. These is a huge amount of possibilities to be investigated as tori interactions or oscillations can be associated to a variety of phenomena with relevant energy release, as we have also partially faced here. Accretion or collision constitute possible scenario for the entire ringed disk instability eventually leading to interesting observational effects. Tori in ringed disk may collide and merge, or, eventually the accreting matter from the outer torus of the couple can impact on the inner torus, or the outer torus may be inactive with an active inner torus accreting onto the **BH**, or both tori may be active. These multi-configurations may be at the root of phenomena eventually detectable by X-ray detectors as the shape of X-ray emission spectra, the X-ray obscuration and absorption by one of the torus, in the extremely energetic radiative phenomena in quasar and **AGNs**. Signatures of **RADs** may be found in the emission shape lines as peaked profiles of radially stratified emission[35,34,36]. The radially oscillating tori of the ringed disk could be related to the high-frequency quasi periodic oscillations observed in non-thermal X-ray emission from compact objects (QPOs), a still obscure feature of the X-ray astronomy related to the inner parts of the disk. Relatively indistinct excesses of the relativistically broadened emission-line components were predicted in difference works, arising in a well-confined radial distance in the accretion structure originating by a series of episodic accretion events. Our analysis first shows that occurrence of these situations is strictly constrained by the black hole spin. This aspect has also important implications on the possible observational effects providing a perspective on the phenomena emerging from their dynamics, isolating those situations where actually these configurations may be chased.

D. P. acknowledges support from the Junior GACR grant of the Czech Science Foundation No:16-03564Y. Z. S. acknowledges the Albert Einstein Centre for Gravitation and Astrophysics supported by grant No. 14-37086G.

A Corotating tori in the ergoregion: RAD tori separation and constraints

The possibility that corotating toroidal extended matter configurations could be formed in the outer ergoregion ("all-contained" accretion tori), Σ_ϵ^+, and even to cross the outer ergosurface, r_ϵ^+, has been investigated in [26]. This situation was then explored in the **RAD** context, particularly in relation to the **RAD** tori separation in corotating tori sub-sequences of **RAD** components (which are possible to form in Σ_ϵ^+), and the counterrotating ones, confined in the outer region of the boundary r_ϵ^+, in dependence on the Kerr **BH** spin–[27,28,32]. Fundamental differences between slow rotating **SMBHs** and faster spinning **SMBHs** were observed. The tori separation is a particularly relevant phenomenon for faster spinning **BHs**. For these spacetimes, quiescent and accreting tori solution of the Euler equation (6), located entirely in Σ_ϵ^+ are possible, proving that, as in Fig. (16), different classes of faster spinning **SMBHs** provide different topological constraints (equilibrium conditions)

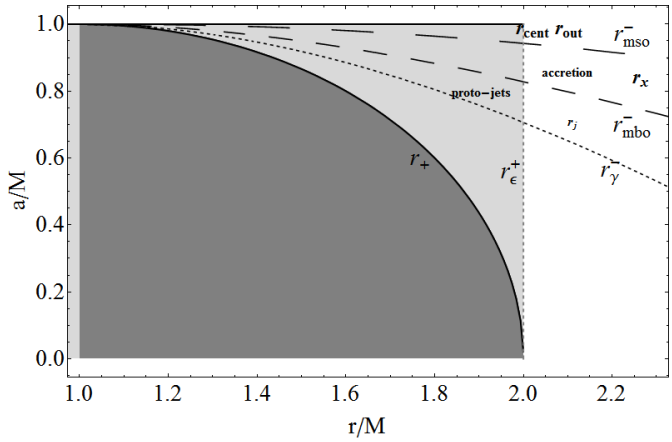

Fig. 16. The outer ergoregion $\Sigma^+_\epsilon \equiv]r_+, 2M]$ (light-gray region) of the Kerr geometry. Gray region is $r < r_+$, r_+ is the **BH** horizon. $r^+_\epsilon = 2M$ is the outer ergosurface. Location of inner edge of quiescent tori and tori center, the region of inner edge of accreting tori $r_\times$ and proto-jets are shown.

for the tori. In [28,32] in particular, this aspect was addressed in relation to the role of ergoregion in the emission and the structure of the proto-jets, whereas a more attentive look to the attractors classification was considered in [30]. To complete the discussion on $n = 2$ **RAD**, we briefly mention the possibility of the ergosurface penetration and all-contained accretion tori (or "dragged surfaces"). The tori location with respect to the central **BH**, with specification on their equilibrium states, are represented in Fig. (16), where the critical points of the hydrostatic pressure are also shown. Clearly, this analysis concerns the case of couple with an inner corotating torus, in accretion or not, i.e. all the couples $()^- < ()^\pm$ are considered according to the constraints and restrictions discussed in Sec. (2). The inner configuration containing or crossing the ergosurface (in the sense illustrated in [26]) can be a "screening torus", as considered in several analysis of the X-ray emission[12,13,14,15,17]. Finally, these tori should have a special relevance also in the evaluation of collisional effects, considered here in Fig. (14), occurring in Σ^+_ϵ with possible applications to the energy extraction processes assumed to occur from the Lense-.Thirring effect in the Σ^+_ϵ. The role of the dragging effects has been also considered in Sec. (4.3) in the evaluation of the mass-accretion rates for corotating and counterrotating tori in dependence of the **BH** spin.

References

1. S. A. Walker, et al MNRAS, 468, 2 2506-2516 (2017)
2. C. Ricci, *et al.*, MNRAS, 468, 1273 (2017)
3. C. Tadhunter, R. Spence, et al arXiv:1702.02573 [astro-ph.GA] (2017)
4. J. Regan, E. Visbal et al. NatureAstronomy, 1, 0075 (2017)
5. S. McAlpine, et sl MNRAS, 468, (3), 3395-3407 (2017)
6. M. Tucci & M. Volonteri, A&A, 600, A64(2017)
7. F. G. Xie& F. Yuan, APJ, 836, 1, 104 (2017)
8. J. S. Collinson et alMNRAS, 465, 1, 358 (2017)
9. M. L. Parker et al., Nature, 543, 83 (2017)
10. J. Zhang, Z.W. Xue, J.J. He, E.W. Liang & S.N. Zhang, APJ, 807, 1, 51 (2015)
11. G. Bao& Z. Stuchlik, APJ, 400, 163 (1992).
12. S. Marchesi, et al., APJ, 830, 100, 20(2016)
13. R. Gilli, A. Comastri, and G. Hasinger, A&A, 463, 79 (2007)
14. S. Marchesi, et alAPJ, 836, 1, 116 (2017)
15. A. Masini, *et al.*, A&A, 589, A59 (2016)
16. C. DeGraf, A. Dekel, J. Gabor, and F. Bournaud, MNRAS, 466, 1462 (2017)
17. T. Storchi-Bergmann et al.APJ, 835, 2 (2017)
18. Kovář, J., Slaný, P., Stuchlík, Z., et al. 2011, Phys. Rev. D, 84, 084002
19. J. Kovář, O. Kopáček, V. Karas, & Y. Kojima, 2013, Classical and Quantum Gravity, 30, 025010
20. J. Kovář, P. Slaný,, C. Cremaschini, et al. 2014, Phys. Rev. D, 90, 044029
21. J. Kovář, P. Slaný, C. Cremaschini , et al. 2016, Phys. Rev. D, 93, 124055
22. P. Slany, J. Kovar, Z. Stuchlik and V. Karas, Astrophys. J. Suppl. **205**, 3 (2013).
23. J. Kovar, P. Slany, Z. Stuchlik, V. Karas, C. Cremaschini and J. C. Miller, Phys. Rev. D **84**, 084002 (2011).
24. K. Schroven, A. Trova, E. Hackmann and C. Lämmerzahl, Phys. Rev. D **98** no.2, 023017 (2018).
25. A. Trova, K. Schroven, E. Hackmann, V. Karas, J. Kovar and P. Slany, Phys. Rev. D **97**, no.10, 104019 (2018).
26. D. Pugliese, & G. Montani, Phys. Rev. D, 91, 083011 (2015)
27. D. Pugliese& Z. Stuchlík, APJS, 221, 2, 25 (2015)
28. D. Pugliese& Z. Stuchlík, APJS, 223, 2, 27(2016)
29. D. Pugliese& Z. Stuchlík, APJS, 229, 2, 40(2017)
30. Pugliese, D., & Stuchlík, Z. 2018, Classical and Quantum Gravity, 35, 185008
31. Pugliese, D., & Stuchlík, Z. 2018, Classical and Quantum Gravity, 35, 105005
32. D. Pugliese& Z. Stuchlík, JHEAp **17** 1 (2018)
33. D. Pugliese and G. Montani, arXiv:1802.07505 [astro-ph.HE].
34. V. Sochora, V. Karas, J. Svoboda, & M. Dovciak, MNRAS, 418, 276–283 (2011)
35. V. Karas, &V. Sochora, APJ, 725, 2, 1507–1515 (2010)
36. J. Schee, & Z. Stuchlík, Gen. Rel. Grav., 41, 1795 (2009)
37. J. Schee, & Z. Stuchlík, JCAP, 2013 (2013)
38. C. Nixon, A. King, D. Price, J. Frank, APJ, 757, L24 (2012)
39. M. Ansorg, A. Kleinwachter, & R. Meinel, MNRAS, 339, 515-523 (2003)
40. C. Alig, M. Schartmann, A. Burkert, K. Dolag, APJ, 771, 2, 119 (2013)
41. R. V. E. Lovelace& T. Chou, APJ, 468, L25 (1996)
42. E. Gafton, E. Tejeda, et al MNRAS, 449, 1, 771 (2015)
43. J. M. Miller, et alNature, 526, 542–545 (2015)
44. P. K. Blanchard, *et al.*, arXiv:1703.07816 [astro-ph.HE] (2017)
45. J.M. Carmona-Loaiza, M. Colpi, M. Dotti& R. Valdarnini, MNRAS, 453, 1608 (2015)
46. S. Dyda, R.V.E. Lovelace, et al MNRAS, 446, 613 (2015)
47. M. Volonteri, F. Haardt, & P. Madau, APJ, 582, 559 (2003)
48. M. Jaroszynski, M. A. Abramowicz, B. Paczynski, Acta Astronm., 30, 1 (1980)
49. B. Paczyński, Acta Astron., 30, 4 (1980)
50. B. Paczyński, & P. Wiita, A&A, 88, 23 (1980)
51. M. Kozłowski, M. Jaroszyński, M. A. Abramowicz, A&A, 63, 209 (1998)
52. M. A. Abramowicz & P. C. Fragile, Living Rev. Relativity, 16, 1 (2013)
53. R. Shafee,J. C, McKinney, et al.APJ, 687, L25 (2008)

54. P. C. Fragile, O. M. Blaes, P. Anninois, & J. D. Salmonson, APJ, 668, 417–429 (2007)
55. J-P. De Villiers, & J. F. Hawley, APJ, 577, 866 (2002)
56. Z. Stuchlík, P. Slaný, & J. Kovar, Class. Quantum Gravity, 26, 215013 (2009)
57. O. Porth, et al.arXiv:1611.09720 [GRqc] (2016)
58. J. A. Font, & F. Daigne, APJ, 581, L23–L26 (2002)
59. J. F. Hawley, APJ, 356, 580 (1990)
60. J. F. Hawley, MNRAS, 225, 677 (1987)
61. J. F. Hawley, APJ, 381, 496 (1991)
62. J. F. Hawley, L. L. Smarr, J. R. Wilson, APJ, 277, 296 (1984)
63. J. A. Font, Living Rev. Relat., 6, 4 (2003)
64. Q. Lei, M. A. Abramowicz, P. C. Fragile, et al.A&A, 498, 471 (2008)
65. R. H. Boyer, Proc. Camb. Phil. Soc., 61, 527 (1965)
66. J. Frank, A. King, D. Raine, *Accretion Power in Astrophysics*, (Cambridge University Press, Cambridge 2002)
67. D. Pugliese, G. Montani,& M. G. Bernardini, MNRAS, 428, 952 (2012)
68. D. Pugliese, & G. Montani, Europhys. Lett., 101, 19001 (2013)
69. H. Kucakova, P. Slany, Z. Stuchlík, JCAP, 01, 033(2011)
70. Rezzolla, L., Zanotti, O., Font, J. A. 2003 A&A, 412, 603
71. Z. Stuchlík, Slaný, P., Torok, G., Abramowic, M. A. 2005, Phys. Rev. D, 71, 2
72. Slaný, P. & Z. Stuchlík 2005 Class. Quantum Gravity, 22, 3623
73. Z. Stuchlík& Slaný, P. 2006, AIP Conf. Proc. 861, 770
74. Z. Stuchlík, Slaný P., Hledík S. 2000, A&A, 363, 425
75. Z. Stuchlík, & J. Kovář, 2008, Int. J. Mod Phys D, 17
76. M. A. Abramowicz, Acta. Astron., 21, 81(1971)
77. S. K. Chakrabarti, MNRAS, 245, 747 (1990)
78. S. K. Chakrabarti, MNRAS, 250, 7 (1991)
79. M. A. Abramowicz, arXiv:astro-ph/0812.3924 (2008)
80. Z. Stuchlik, A. Kotrlova, and G. Torok, A&A, 552, A10 (2013)
81. D. Pugliese, H. Quevedo, & R. Ruffini, Phys. Rev. D, 83, 024021 (2011)
82. D. Pugliese, H. Quevedo, & R. Ruffini, Phys. Rev. D, 84, 044030 (2011)
83. D. Pugliese, H. Quevedo, & R. Ruffini, Phys. Rev. D, 88, 2, 024042 (2013)
84. D. Pugliese& J. A. V. Kroon, Gen. Rel. Grav., 44, 2785 (2012)
85. J. H. Krolik& J. F. Hawley, APJ, 573, 754 (2002)
86. B. C. Bromley, W. A. Miller, V. I. Pariev, Nature, 391, 54, 756 (1998)
87. E. Agol& J. Krolik, APJ, 528, 161 (2000)
88. N. Afshordi& B. Paczynski, Astrophys. J. 592, 354 (2003)
89. D. Pugliese, & H. Quevedo, Eur. Phys. J. C, 75, 5, 234 (2015)
90. Z. Stuchlik, & S. Hledík, K.Truparová Class. Quant. Grav., 28, 15, 155017 (2011).
91. T. Harada, & M. Kimura, Phys. Rev. D, 83, 024002 (2011)
92. A. Tursunov, M. Kolos, A. Abdujabbarov, B. Ahmed, Z. Stuchlik, Phys. Rev. D, 88, 124001 (2013)
93. Z. Stuchlik, Bulletin of the Astronomical Institutes of Czechoslovakia, 31, 129 (1980)
94. M. Blaschke and Z. Stuchlik, Phys. Rev. D **94** 8, 086006 (2016).
95. Z. Stuchlik, & J. Schee, Class. Quant. Grav., 30, 075012 (2013)
96. Z. Stuchlík, & J. Schee, Class. Quant. Grav., 29, 065002 (2012)
97. Z. Stuchlík, M. Blaschke and J. Schee, Phys. Rev. D 96, 10, 104050 (2017)
98. M. Volonteri, M. Sikora, J.-P. Lasota, APJ, 667, 704 (2007)
99. M. Volonteri, APJ, 663, L5 (2007)
100. M.Volonteri, A&AR, 18, 279 (2010)
101. L. X. Li., MNRAS, 424, 1461 (2012).
102. T. Oka, S. Tsujimoto, et al.Nature Astronomy-Letter, (2017)
103. N. Kawakatu, K. Ohsuga, MNRAS, 417, 4, 2562-2570 (2011)
104. S. W. Allen, et al MNRAS, 1, 372, 21 (2006)
105. M. A. Abramowicz, Astronomical Society of Japan, 37, 4, 1985, 727-734
106. M. Middleton, J. Miller-Jones and R. Fender, MNRAS, 439,2, 1740 (2014)
107. R. W. Nelson *et al.*, APJ, 488, L117 (1997)
108. C. J. Nixon, P. J. Cossins, A. R. King, J. E. Pringle, MNRAS, 412, 3, 1591-1598 (2011)
109. C. Roedig and A. Sesana, MNRAS, 439, 4, 3476 (2014).
110. J. A. Font, & F. Daigne, MNRAS, 334, 383 (2002)
111. C. Nixon, A. King, & D. Price, D., MNRAS, 434, 1946 (2013).
112. S. Dogan, C. Nixon, A. King, D. J. Price, MNRAS, 449, 2, 1251 (2015)
113. C. Bonnerot,E. M. Rossi, G. Lodato & D. J. Price, MNRAS, 455, 2, 2253 (2016)
114. I. A. Bonnell, & W. K. M. Rice, Science, 321, 1060 (2008).
115. K. Zubovas, A. King,arXiv:1901.02224 [astro-ph.GA], (2008)
116. H. Aly, W. Dehnen, C. Nixon, & A. King, MNRAS, 449, 1, 65 (2015).
117. M. A. Abramowicz, M. Calvani, & L. Nobili, Nature302, 597–599 (1983).
118. E. Berti, V. Cardoso, L. Gualtieri et al.Phys. Rev. Letter, 103, 239001 (2009).
119. P. G. Jonker, M. A. P. Torres, A. C. Fabian et al.MNRAS, 407, (1), 645-650 (2010).